RL-TR-96-124
Final Technical Report
December 1996

QUASI-OPTIMAL PROCESSING IN SPREAD SPECTRUM ENVIRONMENTS

Illinois Institute of Technology

Donald R. Ucci, William R. Jacklin, and John Tanas

DTIC QUALITY INSPECTED 3

19970224 094

Rome Laboratory
Air Force Materiel Command
Rome, New York

Although this report references documents, (*) listed on page 84, no limited information has been extracted.

This report has been reviewed by the Rome Laboratory Public Affairs Office (PA) and is releasable to the National Technical Information Service (NTIS). At NTIS it will be releasable to the general public, including foreign nations.

RL-TR-96-124 has been reviewed and is approved for publication.

APPROVED:
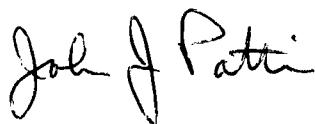
JOHN J. PATTI
Project Engineer

FOR THE COMMANDER:
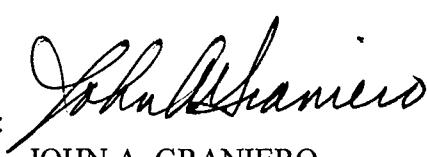
JOHN A. GRANIERO
Chief Scientist
Command, Control & Communications Directorate

REPORT DOCUMENTATION PAGE

Form Approved
OMB No. 0704-0188

1. AGENCY USE ONLY (Leave Blank)	2. REPORT DATE	3. REPORT TYPE AND DATES COVERED
	December 1996	Final Apr 93 – Apr 94

4. TITLE AND SUBTITLE	5. FUNDING NUMBERS
QUASI-OPTIMAL PROCESSING IN SPREAD SPECTRUM ENVIRONMENTS	C – F30602-93-C-0099 PE – 62702F
6. AUTHOR(S) Donald R. Ucci William R. Jacklin John Tanas	PR – 4519 TA – 42 WU – PD

7. PERFORMING ORGANIZATION NAME(S) AND ADDRESS(ES)	8. PERFORMING ORGANIZATION REPORT NUMBER
Illinois Institute of Technology Dept. of Electrical and Computer Engineering Chicao IL 60616	N/A

9. SPONSORING/MONITORING AGENCY NAME(S) AND ADDRESS(ES)	10. SPONSORING/MONITORING AGENCY REPORT NUMBER
Rome Laboratory/C3BB 525 Brooks Rd Rome NY 13441-4505	RL-TR-96-124

11. SUPPLEMENTARY NOTES

Rome Laboratory Project Engineer: John Patti/C3BB/(315)330-3615

12a. DISTRIBUTION/AVAILABILITY STATEMENT	12b. DISTRIBUTION CODE
Approved for Public Release; Distribution Unlimited.	

13. ABSTRACT (Maximum 200 words)

The derivations of robust Locally Optimum (LO) detection algorithms (high interference/signal ratios) with and without memory, and their performance in a spread spectrum communications system, are the subject of this report. There are three forms of LO detection considered: (1) detection with memory; (2) detection in independent and identically distributed (iid) noise; and (3) memoryless detection. Several algorithms are investigated, all using the usual assumption that the small signal corrupting the noise estimate is acceptable. Simulation results show, however, that this assumption is not always valid, even in high interference/ signal ratio environments. Detailed investigations focused on regions of poor performance, using "ideal" signal-free estimates of the noise as a baseline.
The ideal estimator yielded a truly robust detector over a wide range of scenarios. Recommended research should thus be focused on means for obtaining true noise estimates in practical environments.

14. SUBJECT TERMS		15. NUMBER OF PAGES
Communications, Signal processing, Signal detection, Spread spectrum		92
		16. PRICE CODE

17. SECURITY CLASSIFICATION OF REPORT	18. SECURITY CLASSIFICATION OF THIS PAGE	19. SECURITY CLASSIFICATION OF ABSTRACT	20. LIMITATION OF ABSTRACT
UNCLASSIFIED	UNCLASSIFIED	UNCLASSIFIED	UL

NSN 7540-01-280-5500

Standard Form 298 (Rev. 2-89)
Prescribed by ANSI Std. 239-18
298-102

Contents

List of Figures

2

3

List of Tables

Executive Summary

Many military, and commercial, communication systems operate in environments containing large non-Gaussian interference. This interference may be hostile, as in the case of intentional jamming, or friendly, such as co-channel interference. Robust *locally optimum* (LO) detection is one means by which interference exhibiting a large *jammer-to-signal ratio* (J/S) can be mitigated. The term *robust*, in this context, indicates that prior information regarding the channel statistics is not required. Instead, the required LO nonlinearity is implemented using an estimate of the channel noise *probability density function* (pdf). Thus, the robust LO detector can be used in applications where the channel interference is unknown and possibly nonstationary.

The derivations of robust LO detection algorithms with and without memory, and their performance in a communications system, are the subject of this report. There are three forms of LO detection considered: (1) detection with memory, (2) detection in *independent and identically distributed* (iid) noise, and (3) memoryless detection. A number of algorithms for implementing the various detector structures are presented, and include: (1) the univariate and multivariate histogram algorithms, (2) the *M-interval polynomial approximation* (MIPA), (3) the *continuous polynomial approximation* (CPA), (4) the *Fourier series approximation* (FSA), and (5) the univariate and multivariate kernel algorithms. In all of these methods, observed samples of the channel noise are used to estimate the noise pdf, from which an estimate of the LO nonlinearity is constructed. However, in most applications uncorrupted noise samples are unavailable since *the noise is corrupted by the information signal*. A common solution is to employ the large J/S assumption that *the noise pdf is approximately equal to the received signal pdf*. However, simulation results show that this assumption is not always valid, even in high J/S environments.

7

To determine the cause of the observed regions of poor performance, two "ideal" detector structures were examined: (1) the *globally optimum* (GO), and (2) the *ideal LO* (ILO) detectors. In both of these detector algorithms, uncorrupted noise samples, although unavailable in practice, were provided and used to estimate the required noise pdfs. The simulation results showed that both of these techniques provided "robust" performance over a wide range of jamming scenarios. It can be *inferred*, therefore, that robust LO detection techniques will be extremely useful in applications characterized by unknown, nonstationary interference, provided that it is possible to accurately estimate the noise pdf. As a result, techniques for either obtaining uncorrupted estimates of the noise samples, or for constructing an accurate estimate of the noise pdf from a preliminary estimate of the received signal pdf, will be required in order to take full advantage of the "robustness" available in the robust LO detector.

Chapter 1

Introduction

Many military, and commercial, communication systems operate in environments containing large non-Gaussian interference. This interference may be hostile, as in the case of intentional jamming, or friendly, such as co-channel interference. In either case, a performance degradation will likely be observed, even in systems employing standard *spread spectrum* (SS) signaling techniques, since the linear receiver structure commonly used is optimum only in the case of Gaussian channel noise.

One method for improving system performance which has received considerable attention, particularly for applications in high *jammer-to-signal ratio* (J/S) environments, is *locally optimum* (LO) detection [1]-[4]. In its original form, the LO detector utilizes a nonlinearity derived as an approximation to the optimum *maximum likelihood* (ML) detector. In many scenarios, the LO detector is simpler to implement than the corresponding ML detector, and its performance asymptotically approaches that of the ML detector as the signal becomes small relative to the interference.

One drawback to the original form of the LO detector is that, similar to the ML detector, it requires *a priori* knowledge of the noise *probability density function* (pdf) to implement the LO nonlinearity. In most applications of interest, however, the noise statistics are unknown, and possibly nonstationary. Thus, recent efforts have focused on *robust* LO detection techniques [5]-[10], in which the required LO nonlinearity is constructed using estimates of the interference statistics, most notably the pdf and its derivative. Since the robust LO detector implementation is based on estimation techniques, it can adapt to the unknown noise, and modify its structure as the noise

changes.

The derivations of robust LO detection algorithms with and without memory, and their performance in a communications system, are the subject of this report. The organization of the report is as follows. The derivations of the various LO detector algorithms for quadrature signaling are presented in Chapter 2, with an emphasis on *direct sequence* (DS) SS systems. Next, a number of memoryless robust LO detector methods are discussed in Chapter 3. These methods are based on histogram, polynomial, Fourier series, and kernel estimates of the noise magnitude pdf. Results are presented which show the performance characteristics for the various detector algorithms when subjected to a single *continuous wave* (CW) jammer. Algorithms for implementing the robust LO detector with memory are the subject of Chapter 4, and are based on estimating the joint multivariate pdf of the channel noise. Results are also presented for detection in various CW jammer scenarios. While the robust LO detectors discussed in Chapters 3 and 4 require estimates of the noise pdf, the large J/S assumption that the noise pdf is approximately equal to the received signal pdf is used in simulation, since uncorrupted noise observations are typically unavailable in a communications system. The effects of this assumption are investigated in Chapter 5 through the examination of two "ideal" detector algorithms. Finally, the overall conclusions of this research effort are detailed in Chapter 6 of this document.

Chapter 2

Derivation of the Robust LO Detectors for Quadrature Signaling

In quadrature signaling techniques, the information signal is transmitted over two orthogonal channels, namely the *in-phase* (I) and *quadrature* (Q) channels. At baseband, these signals can be represented as a complex waveform given by [11]

$$s_m(t) = s_{I_m}(t) + j s_{Q_m}(t), \ m = 1, \ldots, M, \tag{2.1}$$

where $s_{I_m}(t)$ and $s_{Q_m}(t)$ are T second duration signals transmitted on the I and Q channels, respectively. M denotes the number of different possible signal pairs. Sampling at a rate $f_s = 1/T_s$ produces the vector $\mathbf{s}_m$, written as

$$\mathbf{s}_m = \mathbf{s}_{I_m} + j\mathbf{s}_{Q_m} \tag{2.2}$$

where $\mathbf{s}_m$, $\mathbf{s}_{I_m}$, and $\mathbf{s}_{Q_m}$ are vectors of length N, and $N = T/T_s$. As an example, consider baseband *quadrature phased shift keyed* (QPSK) signaling.

The possible transmitted signal pairs are

$$s_{I_m}(k) + j s_{Q_m}(k) = \sqrt{\frac{E_b}{T}} \begin{cases} 1 + j1 \\ 1 - j1 \\ -1 + j1 \\ -1 - j1 \end{cases} , \ k = 1, \ldots, N \qquad (2.3)$$

where $E_b \doteq \frac{1}{2} \int_0^T |s_m(t)|^2 \, dt$ is the energy in each signal period. The corresponding QPSK signal constellation is shown in Fig. 2.1.
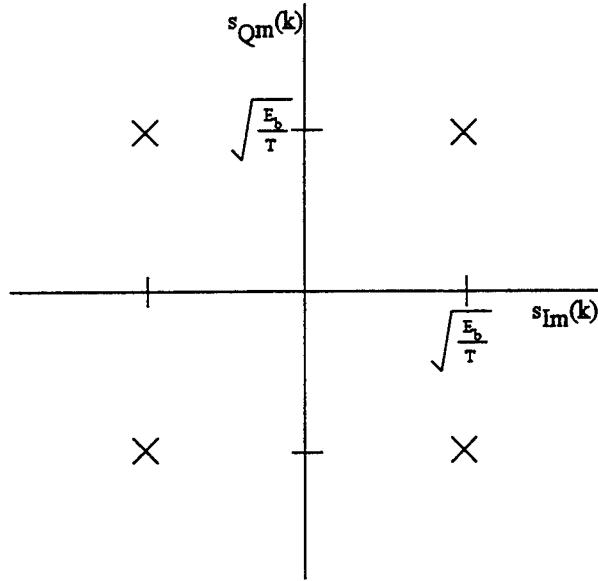
Figure 2.1: QPSK signal constellation

The derivation of the LO detectors for quadrature signaling is as follows: Let the received signal vector of length N be given by

$$\mathbf{r}_I + j\mathbf{r}_Q = \mathbf{s}_{I_m} + \mathbf{n}_I + j(\mathbf{s}_{Q_m} + \mathbf{n}_Q) \qquad (2.4)$$

where M is the number of possible transmitted signal pairs, and $\mathbf{n}_I$ and $\mathbf{n}_Q$ are the I and Q noise vectors (jamming plus background interference). If

the observed value of the received signal is $\rho_I + j\rho_Q$, and the transmitted signal and noise are independent, then from [5] the *maximum likelihood* (ML) detector for this scenario is given by:

Choose the transmitted signal pair, (s_{I_m}, s_{Q_m}), which maximizes

$$\ln[f_{\mathbf{n}_I \mathbf{n}_Q}(\rho_I - s_{I_m}, \rho_Q - s_{Q_m})],$$

(2.5)

where $f_{\mathbf{n}_I \mathbf{n}_Q}(\eta_I, \eta_Q)$ is the joint *probability density function* (pdf) of the noise. Approximating Eq. (2.5) using first-order Taylor series expansions yields the following result:

$$
\begin{aligned}
\ln[f_{\mathbf{n}_I \mathbf{n}_Q}(\rho_I - s_{I_m}, \rho_Q - s_{Q_m})] \;\approx\; & \ln[f_{\mathbf{n}_I \mathbf{n}_Q}(\rho_I, \rho_Q)] \\
& - \sum_{k=1}^{N} \left[s_{I_m}(k) \tfrac{\partial}{\partial \rho_I(k)} \ln[f_{\mathbf{n}_I \mathbf{n}_Q}(\rho_I, \rho_Q)] \right. \\
& \left. + s_{Q_m}(k) \tfrac{\partial}{\partial \rho_Q(k)} \ln[f_{\mathbf{n}_I \mathbf{n}_Q}(\rho_I, \rho_Q)] \right].
\end{aligned}
$$

(2.6)

Since the term $\ln[f_{\mathbf{n}_I \mathbf{n}_Q}(\rho_I, \rho_Q)]$ is constant for all m, the ML detector can be approximated by:

Choose the transmitted signal pair, (s_{I_m}, s_{Q_m}), which maximizes

$$
\begin{aligned}
l(\rho) = l(\rho_I, \rho_Q) \;=\; & - \sum_{k=1}^{N} \left[s_{I_m}(k) \tfrac{\partial}{\partial \rho_I(k)} \ln[f_{\mathbf{n}_I \mathbf{n}_Q}(\rho_I, \rho_Q)] \right. \\
& \left. + s_{Q_m}(k) \tfrac{\partial}{\partial \rho_Q(k)} \ln[f_{\mathbf{n}_I \mathbf{n}_Q}(\rho_I, \rho_Q)] \right] \qquad (2.7)
\end{aligned}
$$

$$
= \; s_{I_m}^T g_I(\rho_I, \rho_Q) + s_{Q_m}^T g_Q(\rho_I, \rho_Q),
$$

where $g_I(\rho_I, \rho_Q) = [g_{I_1}(\rho) \ldots g_{I_N}(\rho)]^T$, $g_Q(\rho_I, \rho_Q) = [g_{Q_1}(\rho) \ldots g_{Q_N}(\rho)]^T$, and

$$
g_{I_k}(\rho) \;\doteq\; -\frac{\partial}{\partial \rho_I(k)} \ln[f_{\mathbf{n}_I \mathbf{n}_Q}(\rho_I, \rho_Q)] = -\frac{\frac{\partial}{\partial \rho_I(k)} f_{\mathbf{n}_I \mathbf{n}_Q}(\rho_I, \rho_Q)}{f_{\mathbf{n}_I \mathbf{n}_Q}(\rho_I, \rho_Q)}
$$

(2.8)

$$
g_{Q_k}(\rho) \;\doteq\; -\frac{\partial}{\partial \rho_Q(k)} \ln[f_{\mathbf{n}_I \mathbf{n}_Q}(\rho_I, \rho_Q)] = -\frac{\frac{\partial}{\partial \rho_Q(k)} f_{\mathbf{n}_I \mathbf{n}_Q}(\rho_I, \rho_Q)}{f_{\mathbf{n}_I \mathbf{n}_Q}(\rho_I, \rho_Q)}.
$$

(2.9)

The functions $g_{I_k}(\rho)$ and $g_{I_k}(\rho)$ of Eq. (2.8) and Eq. (2.9) are called the LO nonlinearities with memory, and Eq. (2.7) describes the LO detector with memory.

The LO detector of Eq. (2.7) can be greatly simplified if the noise samples are *independent and identically distributed* (iid). In this case, the joint pdf of the channel noise becomes

$$f_{n_I n_Q}(\boldsymbol{\eta}_I, \boldsymbol{\eta}_Q) = \prod_{k=1}^{N} f_{n_I n_Q}(\eta_I(k), \eta_Q(k)). \qquad (2.10)$$

The LO nonlinearities of Eq. (2.8) and Eq. (2.9) then become

$$g_{I_k}(\boldsymbol{\rho}) = g_I(\rho_I, \rho_Q) = -\frac{\partial}{\partial \rho_I} \ln[f_{n_I n_Q}(\rho_I, \rho_Q)] = -\frac{\frac{\partial}{\partial \rho_I} f_{n_I n_Q}(\rho_I, \rho_Q)}{f_{n_I n_Q}(\rho_I, \rho_Q)} \qquad (2.11)$$

$$g_{Q_k}(\boldsymbol{\rho}) = g_Q(\rho_I, \rho_Q) = -\frac{\partial}{\partial \rho_Q} \ln[f_{n_I n_Q}(\rho_I, \rho_Q)] = -\frac{\frac{\partial}{\partial \rho_Q} f_{n_I n_Q}(\rho_I, \rho_Q)}{f_{n_I n_Q}(\rho_I, \rho_Q)}, \qquad (2.12)$$

where $\rho_I \doteq \rho_I(k)$ and $\rho_Q \doteq \rho_Q(k)$. Thus, the $2N$-variate functions of Eq. (2.8) and Eq. (2.9) reduce to the functions of 2 variables given by Eq. (2.11) and Eq. (2.12). Finally, the LO detector of Eq. (2.7) becomes:

Choose the transmitted signal pair, (s_{I_m}, s_{Q_m}), which maximizes

$$l(\rho_I, \rho_Q) = -\sum_{k=1}^{N} \left[s_{I_m}(k) \frac{\partial}{\partial \rho_I(k)} \ln[f_{n_I n_Q}(\rho_I(k), \rho_Q(k))] \right. \\ \left. + s_{Q_m}(k) \frac{\partial}{\partial \rho_Q(k)} \ln[f_{n_I n_Q}(\rho_I(k), \rho_Q(k))] \right]. \qquad (2.13)$$

Further simplification of the LO detector results if the channel noise samples are iid and if the joint pdf has bivariate radial symmetry. Under this assumption, the joint noise pdf can be written as

$$f_{n_I n_Q}(\eta_I, \eta_Q) = \begin{cases} f_n(\eta)/(2\pi\eta), & 0 \le \theta_n < 2\pi \\ \\ 0, & \text{otherwise} \end{cases} \qquad (2.14)$$

where $f_n(\eta)$ is the envelope pdf of the noise, $n = \sqrt{n_I^2 + n_Q^2}$ is the magnitude of the noise, and $\theta_n = \tan^{-1}(n_Q/n_I)$ is the phase of the noise. The radial symmetry assumption is valid for many interference sources of interest as they have random phase angles. Even a constant frequency waveform will have a vector that rotates at a uniform rate relative to the transmitted signal vector,

14

and is therefore equally likely at any angle [10]. Under this assumption, the LO detector of Eq. (2.13) becomes the memoryless LO detector, and is given by:

Choose the transmitted signal pair, (s_{I_m}, s_{Q_m}), which maximizes

$$l(\rho_I, \rho_Q) = \sum_{k=1}^{N} [s_{I_m}(k)g(\rho(k))\cos(\theta_r(k)) \qquad (2.15)$$
$$+s_{Q_m}(k)g(\rho(k))\sin(\theta_r(k))]$$

where

$$g(\rho(k)) \doteq -\frac{d}{d\rho(k)}\ln[f_n(\rho(k))] + \frac{1}{\rho(k)} = -\frac{\frac{d}{d\rho(k)}f_n(\rho(k))}{f_n(\rho(k))} + \frac{1}{\rho(k)}, \quad (2.16)$$

$\rho(k) = \sqrt{\rho_I^2(k) + \rho_Q^2(k)}$ is the observed magnitude of the received signal, and $\theta_r(k) = \tan^{-1}(\rho_Q(k)/\rho_I(k))$ is the observed phase.

A discussion of the LO nonlinearity is necessary at this point. In deriving the approximation of the joint noise pdf in Eq. (2.6), an important assumption was made, namely the *small signal assumption*. Since only the first-order Taylor series was used to approximate $\ln[f_{n_I n_Q}(\cdot)]$ in Eq. (2.6), it is necessary that the higher order terms of the Taylor series decay to zero. These higher order terms all contain powers of $s_{I_m}(k)$ and $s_{Q_m}(k)$. If $| s_{I_m}(k) | \ll 1$ and $| s_{Q_m}(k) | \ll 1$, then $[s_{I_m}(k)]^p$, $[s_{Q_m}(k)]^p$, and $[s_{I_m}(k)]^{p_1}[s_{Q_m}(k)]^{p_2}$ all approach zero, and the higher order terms of the Taylor series become negligible.

The small signal assumption is also equivalent to the large *jammer-to-signal ratio* (J/S) assumption, i.e., that the noise is much larger than the information signal. To see this, assume that $| n | \gg | s |$, where n is the random noise variable and s is the information signal. Let $\tilde{n} = n/A$ and $\tilde{s} = s/A$, where $A > 0$ is chosen such that $| s | \ll 1$. If the pdf of n is $f_n(\eta)$ and the pdf of $\tilde{n}$ is $f_{\tilde{n}}(\tilde{\eta})$, then $f_{\tilde{n}}(\tilde{\eta}) = Af_n(A\tilde{n})$ [12]. Note that if η is the observation of n, then $\tilde{\eta}$ is the observation of $\tilde{n}$, where $\tilde{\eta} = \eta/A$. The LO nonlinearity corresponding to $f_n(\eta)$ is $g(\rho) = -f_n'(\rho)/f_n(\rho) + 1/\rho$, where $(')$ denotes differentiation. The LO nonlinearity corresponding to $f_{\tilde{n}}(\tilde{\eta})$ is $\tilde{g}(\tilde{\rho}) = -f_{\tilde{n}}'(\tilde{\rho})/f_{\tilde{n}}(\tilde{\rho}) + 1/\tilde{\rho} = -Af_n'(A\tilde{\rho})/f_n(A\tilde{\rho}) + 1/\tilde{\rho} = Ag(\rho)$, where $\tilde{\rho} = \rho/A$. Since $g(\rho)$, the LO nonlinearity corresponding to the large J/S assumption, and $\tilde{g}(\tilde{\rho})$, the LO nonlinearity corresponding to the small signal assumption, differ by only a constant, the resulting LO detector structures are equivalent.

Thus, the Taylor series approximation of Eq. (2.6) is also valid under the large J/S assumption commonly used in many military communications scenarios.

Of particular interest in this report is the LO detection of QPSK signals in a *direct sequence* (DS) *spread spectrum* (SS) communications system. In the DSSS system shown in Fig. 2.2, the information signal in the ith interval, $[iT, (i+1) \cdot T)$, is given by

$$d(t) = d_m(i)\Pi(t - iT) = [d_{I_m}(i) + jd_{Q_m}(i)]\Pi(t - iT) \qquad (2.17)$$

where $\Pi(t)$ is a unit pulse with a duration of T seconds, and $d_m(i)$ can be one of four ($M = 4$) possible quadrature signals:

$$d_{I_m}(i) + jd_{Q_m}(i) = \begin{cases} 1 + j1 \\ 1 - j1 \\ -1 + j1 \\ -1 - j1 \end{cases} \qquad (2.18)$$

The information signals in the I and Q channels are then multiplied by *psuedo-noise* (PN) "chipping signals," $c_I(t)$ and $c_Q(t)$, respectively, as given by

$$c_{I,Q}(t) = \sqrt{\frac{E_c}{T_c}} \sum_k c_{I,Q}(k)\Pi(t - kT_c) \qquad (2.19)$$

where $E_c = \frac{1}{2}\int_0^{T_c} | c_I(t) + jc_Q(t) |^2 \, dt$ and $c_I(k) = \pm 1$ and $c_Q(k) = \pm 1$ each with probability 1/2. The resulting transmitted signal during the ith interval in the QPSK DSSS system is [1]

$$s(t) = s_I(t) + js_Q(t) = \sqrt{\frac{E_c}{T_c}} \sum_{k=1}^{N} [d_{I_m}(i)c_I(k) + jd_{Q_m}(i)c_Q(k)] \, \Pi(t - kT_c).$$
$$(2.20)$$

The value of N, the length of the signal vectors, is given by $N = T/T_c$ and is the number of chips per information symbol.

---

[1]Note that $d_m(i)$ is constant in the interval $[iT, (i+1) \cdot T)$.
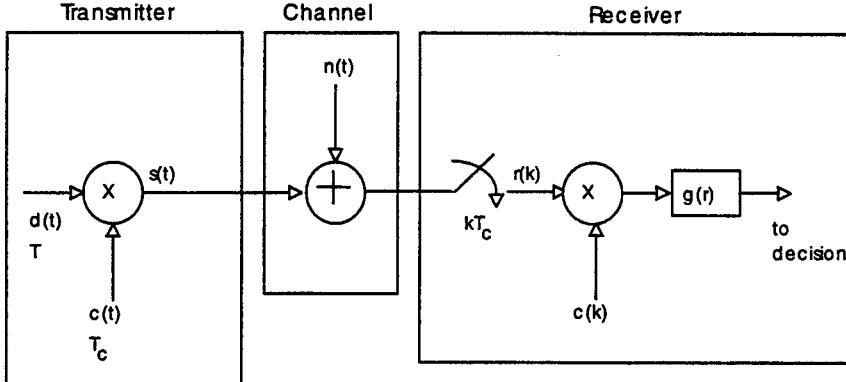
Figure 2.2: A QPSK DSSS communications system with LO detection

As shown in Fig. 2.2, the sampled version of the received signal, $r_I(k) + jr_Q(k)$, in the interval $[iT, (i+1)T)$ is formed by sampling the received signal at T_c seconds [2], yielding the following expression

$$r_I(k) + jr_Q(k) = \sqrt{\frac{E_c}{T_c}}d_{I_m}(i)c_I(k) + n_I(k) + j\left[\sqrt{\frac{E_c}{T_c}}d_{Q_m}(i)c_Q(k) + n_Q(k)\right],$$
$$(2.21)$$

where $n_I(k) + jn_Q(k)$ is the (complex) sampled version of the channel noise. Let the observed value of the received signal be $\rho_I + j\rho_Q$. By analogy to the derivations of the LO detectors at the beginning of this chapter, and removing any constant multipliers, the resulting LO detectors for the QPSK DSSS system are:

Choose the transmitted signal pair, $(d_{I_m}(i), d_{Q_m}(i))$, which maximizes

$$l(\rho_I, \rho_Q) = -\sum_{k=1}^{N}\left[d_{I_m}(i)c_I(k)\frac{\partial}{\partial\rho_I(k)}\ln[f_{n_I n_Q}(\rho_I, \rho_Q)]\right.$$
$$\left. + d_{Q_m}(i)c_Q(k)\frac{\partial}{\partial\rho_Q(k)}\ln[f_{n_I n_Q}(\rho_I, \rho_Q)]\right] \qquad (2.22)$$

---

[2]One can also sample at higher rates. Here, sampling at the chip rate was chosen so as to simplify the notation. The simulation results in subsequent chapters, however, utilize multiple samples per chip.

LO detector with memory

$$l(\rho_I, \rho_Q) = -\sum_{k=1}^{N} \left[d_{I_m}(i) c_I(k) \frac{\partial}{\partial \rho_I(k)} \ln[f_{n_I n_Q}(\rho_I(k), \rho_Q(k))] \right.$$

$$\left. + d_{Q_m}(i) c_Q(k) \frac{\partial}{\partial \rho_Q(k)} \ln[f_{n_I n_Q}(\rho_I(k), \rho_Q(k))] \right] \quad (2.23)$$

LO detector for iid noise

$$l(\rho_I, \rho_Q) = \sum_{k=1}^{N} \{ d_{I_m}(i) c_I(k) g[\rho(k)] \cos[\theta_r(k)] $$

$$+ d_{Q_m}(i) c_Q(k) g[\rho(k)] \sin[\theta_r(k)] \} \quad (2.24)$$

memoryless LO detector

The LO detectors described in Eq. (2.22) to Eq. (2.24) all require knowledge of the noise pdf. However, in most cases of interest this knowledge is either unavailable, or the interference is nonstationary. In these cases, the LO nonlinearities must be estimated, either by estimating the noise pdf, or by estimating the nonlinearity directly. This approach of *robust* LO detection is the subject of the remainder of this report.

Chapter 3

Memoryless LO Detector Implementation Techniques

The preceding chapter presented the derivations of a number of LO detectors. The type of LO detector chosen for a particular application is primarily a consequence of the assumptions made concerning the noise samples. If the noise samples are iid, and their pdf exhibits radial symmetry, then a memoryless LO detector, such as that of Eq. (2.15) and Eq. (2.24) may be used. Once a good model of the noise is obtained, or at least some initial assumptions are determined, the next step is to implement the corresponding LO detector.

In the military environment, since most intentional jamming techniques have an unknown nature, an accurate model of the noise pdf is usually not known *a priori*. In these scenarios, the noise pdf must be estimated from the available data samples. This estimate is then used to implement an approximate LO nonlinearity. If the uncorrupted noise samples are unavailable (as is the usual case in a communications system) and the small-signal assumption is valid, the received signal samples may be used in many cases to give a crude approximation of the noise pdf. Thus, various univariate pdf estimation techniques and their use in implementing the LO detector are discussed in the remainder of this section.

3.1 Review of the Histogram Algorithm

Using the histogram as a means of implementing the memoryless LO non-linearity has been extensively studied in [5] and [6]. Recall that the one-dimensional memoryless LO nonlinearity of Eq. (2.16) can be written as

$$g(\rho_i) \doteq -\frac{d}{d\rho_i}\ln[f_n(\rho_i)] + \frac{1}{\rho_i}. \tag{3.1}$$

To approximate $g(\rho_i)$ using the histogram algorithm, the first step is to approximate $f_n(\rho_i)$. Let $\{\eta_i\}$ be the set of Q observed noise magnitude samples, and divide the range of $\{\eta_i\}$ into K intervals or "bins", B_k, where

$$B_k = \{\eta_i: \quad b_k \le \eta_i < b_{k+1}, \quad k = 0, \ldots, K-1\}. \tag{3.2}$$

The values $\{b_k\}$, with $b_0 = x_{min}$ and $b_K = x_{max}$, are called the "breakpoints" of the histogram and are determined heuristically. For example, the break-points may be chosen so that the bins have equal width, or so that each bin contains the same number of observed samples. Next, the probability of a sample being in each bin, $P\{B_k\}$, is approximated by its relative frequency

$$\hat{P}\{B_k\} = \frac{1}{Q}\sum_{i=1}^{Q} I_{B_k}(\eta_i) \tag{3.3}$$

where $I_A(y)$ is the set indicator function, i.e., $I_A(y) = 1$ for $y \in A$ and 0 otherwise. Then, the histogram estimate of $f_n(\rho_i)$, denoted as $\hat{f}_n(\rho_i)$, is given by

$$\hat{f}_n(\rho_i) = \sum_{k=0}^{K-1} \frac{\hat{P}\{B_k\}}{b_{k+1} - b_k} I_{B_k}(\rho_i). \tag{3.4}$$

Next, the derivative of $\ln[\hat{f}_n(\rho_i)]$ must be computed. If it is assumed that the actual pdf $f_n(\rho_i)$ is continuous, then the impulses that arise from differentiating Eq. (3.4) do not accurately model $\frac{d}{d\rho_i}\ln[f_n(\rho_i)]$. To remedy this dilemma another way of viewing the histogram is utilized. One can think of the process of assigning samples to a bin as a form of quantization. In other words, all ρ_i in the range $(b_k \le \rho_i < b_{k+1})$ are quantized to b_k. Then a numerical approximation of the derivative of $\ln[f_n(\rho_i)]$ evaluated at b_k is

used, i.e.,

$$\frac{\partial}{\partial \rho_i} \ln[f_n(\rho_i)] \mid_{\rho_i = b_k} \approx \frac{\ln[\hat{f}_n(b_{k+1})] - \ln[\hat{f}_n(b_{k-1})]}{b_{k+1} - b_{k-1}}$$

$$\approx \frac{\ln[\hat{P}(B_{k+1})] - \ln[\hat{P}(B_{k-1})]}{b_{k+1} - b_{k-1}} \qquad (3.5)$$

$$- \frac{\ln[b_{k+2} - b_{k+1}] - \ln[b_k - b_{k-1}]}{b_{k+1} - b_{k-1}}.$$

Note, if the bins have equal width then the right side of Eq. (3.5) reduces to $\frac{\ln[\hat{P}\{B_{k+1}\}] - \ln[\hat{P}\{B_{k-1}\}]}{2\Delta}$ where Δ is the width of a bin. Finally, the value of the approximation is extended from b_k to all ρ_i in the range ($b_k \leq \rho_i < b_{k+1}$), yielding the histogram implementation of the memoryless LO nonlinearity:

$$\hat{g}(\rho_i) = - \sum_{k=0}^{K-1} \left\{ \frac{\ln[\hat{P}\{B_{k+1}\}] - \ln[\hat{P}\{B_{k-1}\}]}{2\Delta} \right\} I_{B_k}(\rho_i) + \frac{1}{\rho_i}. \qquad (3.6)$$

Histogram estimation of pdfs usually require a large number of samples ([14], Ch. 3). Thus Q, the total number of observed samples used to construct the histogram, may be much larger than N, the number of samples in each signal vector. To obtain the total number of required observed samples, the value of Q should be chosen such that $Q = CN$, where C is an integer chosen to yield enough samples to construct and accurate histogram. The C vectors can be stored and all the available samples used to compute the histogram. Detection can then be performed on each data vector using the resulting histogram to compute the approximate nonlinearity of Eq. (3.6).

3.2   Review of the MIPA Algorithm

The *M-interval polynomial approximation* (MIPA) is a polynomial-based method for estimating the noise magnitude pdf, $f_n(\eta)$ [5] [9]. In this algorithm the domain of the PDF estimate is divided into M intervals, one for each approximating polynomial.[1] More formally, let $\{\eta_i\}$ be the set of Q observed samples of the noise magnitude random variable, n, and as in the histogram method, divide the range of $\{\eta_i\}$ into M intervals, or "bins,"

---

[1]Note that in this context, M, the number of intervals, is *not* necessarily the same as the number of different possible transmitted signal pairs.

B_k defined by the bin breakpoints $\{b_k\}$ as in Eq. (3.2), where in this case $M = K$. The MIPA estimate, $\hat{f}_n(\eta)$, of the noise pdf can be written as

$$\hat{f}_n(\eta) = \sum_{i=0}^{M-1} \hat{f}_i(\eta) I_{[b_i, b_{i+1})}(\eta) \tag{3.7}$$

where

$$\hat{f}_i(\eta) = a_{i0} + a_{i1}\eta + \cdots + a_{ip}\eta^p \tag{3.8}$$

is the approximating polynomial for the ith bin, p is the MIPA order, and $I_A(y)$ is the set indicator function. The MIPA polynomial coefficients a_{ij} are obtained by first constructing a polynomial approximation of the noise pdf conditioned on the event that the observation η lies in the ith bin. Recall that the conditional noise, $f_{c_i}(\eta)$, for the ith bin can be written as

$$f_{c_i}(\eta) = f_n(\eta \mid b_i \leq \eta < b_{i+1}) = \frac{f_n(\eta)}{P(b_i \leq \eta < b_{i+1})} \tag{3.9}$$

where $P(b_i \leq \eta < b_{i+1})$ is the probability that η is in the interval $[b_i, b_{i+1})$. Let the approximating polynomial, $\hat{f}_{c_i}(\eta)$, for $f_{c_i}(\eta)$ have the form

$$\hat{f}_{c_i}(\eta) = c_{i0} + c_{i1}\eta + \cdots + c_{ip}\eta^p. \tag{3.10}$$

The coefficients c_{ij} are determined by minimizing the *integrated squared error* (ISE) between $\hat{f}_{c_i}(\eta)$ and $f_{c_i}(\eta)$, given by

$$\begin{aligned}
ISE &= \int_{b_i}^{b_{i+1}} \left[f_{c_i}(\eta) - \hat{f}_{c_i} \right]^2 d\eta \tag{3.11} \\
&= \int_{b_i}^{b_{i+1}} \left[f_{c_i}(\eta) - \sum_{j=0}^{p} c_{ij}\eta^j \right]^2 d\eta.
\end{aligned}$$

Taking the derivative of the ISE with respect to c_{ik}, setting it equal to zero, and simplifying yields the following result:

$$\int_{b_i}^{b_{i+1}} f_{c_i}(\eta)\eta^k d\eta = \int_{b_i}^{b_{i+1}} \eta^k \sum_{j=0}^{p} c_{ij}\eta^j d\eta, \quad k = 0, \ldots, p. \tag{3.12}$$

The term on the left side of Eq. (3.12) is the kth moment of $f_{c_i}(\eta)$, i.e., m_{i_k} [12]. Solving the integral on the right side of Eq. (3.12) and writing the result

in matrix form yields the solution for the MIPA coefficients of general order:

$$
\begin{bmatrix} m_{i_0} \\ m_{i_1} \\ \vdots \\ m_{i_p} \end{bmatrix} = \begin{bmatrix} \frac{b_{i+1}-b_i}{1} & \frac{b_{i+1}^2-b_i^2}{2} & \cdots & \frac{b_{i+1}^{p+1}-b_i^{p+1}}{p+1} \\ \frac{b_{i+1}^2-b_i^2}{2} & \frac{b_{i+1}^3-b_i^3}{3} & & \vdots \\ \vdots & & \ddots & \vdots \\ \frac{b_{i+1}^{p+1}-b_i^{p+1}}{p+1} & \cdots & \cdots & \frac{b_{i+1}^{2p+1}-b_i^{2p+1}}{2p+1} \end{bmatrix} \times \begin{bmatrix} c_{i0} \\ c_{i1} \\ \vdots \\ c_{ip} \end{bmatrix} \tag{3.13}
$$

or:

$$
\mathbf{m}_i = \mathbf{H}_i \times \mathbf{c}_i \tag{3.14}
$$

where $\mathbf{c} = [c_{i0}\, c_{i1}\, \ldots\, c_{ip}]^T$ is the polynomial coefficient vector, $\mathbf{m}_i$ is the vector of moments, and $\mathbf{H}_i$ is the matrix of intervals. From this formula $\mathbf{c}_i$ can be computed as

$$
\mathbf{c}_i = \mathbf{H}_i^{-1} \times \mathbf{m}_i . \tag{3.15}
$$

A major drawback of the solution for $\mathbf{c}_i$ in Eq. (3.15) is that the inversion of $\mathbf{H}_i$ is computationally intensive and must be performed for each of the M intervals. However, a significant reduction in computation can be achieved by applying the linear transform

$$
\alpha = \frac{\eta - b_i}{b_{i+1} - b_i} \tag{3.16}
$$

to Eq. (3.12). This expression maps the interval $[b_i, b_{i+1})$ to $[0,1)$. If x_i is the random variable whose outcome is α, then the joint pdf of x_i, $f_{x_i}(\alpha)$, can be written as $f_{x_i}(\alpha_i) = (b_{i+1} - b_i) f_{c_i}((b_{i+1} - b_i)\alpha + b_i)$. Thus, the system of equations in Eq. (3.12) becomes

$$
\int_0^1 f_{x_i}(\alpha)[(b_{i+1}-b_i)\alpha+b_i]^k d\alpha = \sum_{j=0}^p \int_0^1 c_{ij}[(b_{i+1}-b_i)\alpha+b_i]^{j+k} d\alpha, \quad k = 0, \ldots, p.
$$

$$\tag{3.17}$$

Next, examine the following system of equations:

$$
\int_0^1 f_{x_i}(\alpha)\alpha^k d\alpha = \sum_{j=0}^p \int_0^1 d_{ij}\alpha^{j+k} d\alpha, \quad k = 0, \ldots, p. \tag{3.18}
$$

The solution of Eq. (3.18) for $\mathbf{d} = [d_{i0}\, d_{i1}\, \ldots\, d_{ip}]^T$ yields the MIPA estimate, $\hat{f}_{x_i}(\alpha)$, for $f_{x_i}(\alpha)$, namely

$$
\hat{f}_{x_i}(\alpha) = d_{i0} + d_{i1}\alpha + \ldots + d_{ip}\alpha^p \tag{3.19}
$$

where

$$\mathbf{d}_i = \tilde{\mathbf{H}}^{-1} \times \tilde{\mathbf{m}}_i . \tag{3.20}$$

The vector $\tilde{\mathbf{m}}_i$ contains the first p moments of x_i, and $\tilde{\mathbf{H}}$ is a constant matrix (for all i) that is given by

$$\tilde{\mathbf{H}} = \begin{bmatrix} 1 & \frac{1}{2} & \cdots & \frac{1}{p+1} \\ \frac{1}{2} & \frac{1}{3} & \cdots & \frac{1}{p+2} \\ \vdots & & \ddots & \vdots \\ \frac{1}{p+1} & \frac{1}{p+2} & \cdots & \frac{1}{2p+1} \end{bmatrix} \tag{3.21}$$

and needs to be inverted only once. Comparing Eq. (3.17) with Eq. (3.18), it can be shown that the coefficients c_{ij} can be computed from a linear combination of the coefficients d_{ij} []. If $\mathbf{L}_i$ is the corresponding linear transformation matrix, then

$$\mathbf{c}_i = \mathbf{L}_i \times \mathbf{d}_i . \tag{3.22}$$

Thus, the coefficients $\mathbf{a}_i = [a_{i0} \, a_{i1} \, \ldots \, a_{ip}]^T$ for the overall MIPA pdf estimate, $\hat{f}_n(\eta)$, in Eq. (3.7) and Eq. (3.8) can be found as

$$\mathbf{a}_i = \mathbf{L}_i \times \tilde{\mathbf{H}}^{-1} \times \tilde{\mathbf{m}}_i \cdot P(b_i \leq \eta < b_{i+1}) . \tag{3.23}$$

As a final observation, the actual values for the first p moments of x_i are usually unavailable. However, they can be estimated from the available data. Let $\{\eta_{c_j}\}$ be the set of Q_i observations of the noise random variable, n, that lie in the ith bin. If $\tilde{m}_{i_k}$ is the kth moment of x_i, then

$$\hat{m}_{i_k} = \frac{1}{Q_i} \sum_{j=1}^{Q_i} \left(\frac{\eta_{c_j} - b_i}{b_{i+1} - b_i} \right)^k \tag{3.24}$$

can be used to estimate $\tilde{m}_{i_k}$. Defining $\hat{\mathbf{m}}_i$ to be $\hat{\mathbf{m}}_i = [1 \, \hat{m}_{i_1} \, \ldots \, \hat{m}_{i_p}]^T$, since $\tilde{m}_{i_0} = 1$, then the MIPA coefficients in Eq. (3.23) can be computed as

$$\mathbf{a}_i = \mathbf{L}_i \times \tilde{\mathbf{H}}^{-1} \times \hat{\mathbf{m}}_i \cdot P(b_i \leq \eta < b_{i+1}) . \tag{3.25}$$

Once the MIPA coefficient vectors, $\mathbf{a}_i$, $i = 0, \ldots, M-1$, are computed, the resulting MIPA estimate, $\hat{g}(\rho)$, of the memoryless LO nonlinearity is given by

$$\hat{g}(\rho) = -\sum_{i=0}^{M-1} \frac{a_{i1} + 2a_{i2}\rho + \ldots + ja_{ij}\rho^{j-1} + \ldots + pa_{ip}\rho^{p-1}}{a_{i0} + a_{i1}\rho + \ldots + a_{ip}\rho^p} I_{[b_i, b_{i+1})}(\rho) + \frac{1}{\rho}.$$
(3.26)

3.3 The CPA Algorithm

The CPA method of estimating a univariate pdf has been documented in [7] and [8]. This method, like the MIPA algorithm, utilizes a concatenation of polynomials to construct the overall pdf estimate. However, the CPA algorithm also provides an estimate that is continuous and that posseses continuous derivatives, with the degree of continuity determined by the approximation order. Four types of CPA algorithms are discussed in this section: the basic CPA, the *CPA with linear transform* (CPALT), the *CPA with Gaussian tails* (CPAGT), and the *CPA with auxiliary function* (CPAUX).

In the basic CPA algorithm, an estimate of the *cumulative distribution function* (cdf) corresponding to the desired pdf is formed. This estimate is constructed in such a manner so as to have continuous first and second derivatives at all bin breakpoints. The result is a pdf estimate which has a continuous first derivative, a property that is desirable when implementing the memoryless LO nonlinearity. Formally, given $\{\eta_i\}$ as the set of Q observations of the noise magnitude random variable, divide the range of $\{\eta_i\}$ into K bins, B_k, with breakpoints, $\{b_k\}$, defined as in Eq. (3.2). Next, a histogram estimate of the noise cdf is constructed, where the resulting histogram values at the breakpoints $b_0, \ldots, b_K$ are $Y_0, \ldots, Y_K$, with $Y_0 = 0$ and $Y_K = 1$. Then, the basic CPA estimate, $\hat{F}_N(\eta)$, of the noise cdf, $F_n(\eta)$, is given by

$$\hat{F}_n(\eta) = \sum_{i=0}^{K-1} y_i(\eta) I_{[b_i, b_{i+1})}(\eta)$$
(3.27)

where

$$y_i(\eta) = a_{i0} + a_{i1}\eta + \cdots + a_{ip}\eta^p$$
(3.28)

and p is the order of the approximation. The value of p is determined by the number of continuity constraints required in the algorithm. For the basic

25

CPA algorithm with continuous first and second derivatives, $p = 5$, and is determined by using the constraints that $\hat{F}_n(\eta)$ must be continuous and have continuous first and second derivatives at all of the breakpoints [7]. The coefficients $a_{ij}, i = 0, 1, \ldots, K-1$ and $j = 0, 1, \ldots, p$, for $p = 5$ are given by [7]

$$
\begin{bmatrix}
1 & b_{i+1} & b_{i+1}^2 & b_{i+1}^3 & b_{i+1}^4 & b_{i+1}^5 \\
1 & b_i & b_i^2 & b_i^3 & b_i^4 & b_i^5 \\
0 & 1 & 2b_{i+1} & 3b_{i+1}^2 & 4b_{i+1}^3 & 5b_{i+1}^4 \\
0 & 1 & 2b_i & 3b_i^2 & 4b_i^3 & 5b_i^4 \\
0 & 0 & 2 & 6b_{i+1} & 12b_{i+1}^2 & 20b_{i+1}^3 \\
0 & 0 & 2 & 6b_i & 12b_i^2 & 20b_i^3
\end{bmatrix}
\begin{bmatrix}
a_{i0} \\
a_{i1} \\
a_{i2} \\
a_{i3} \\
a_{i4} \\
a_{i5}
\end{bmatrix}
=
\begin{bmatrix}
Y_{i+1} \\
Y_i \\
Y'_{i+1} \\
Y'_i \\
Y''_{i+1} \\
Y''_i
\end{bmatrix}
\qquad (3.29)
$$

where Y_i is the value of the histogram cdf at the ith breakpoint, Y'_i is the approximate derivative of the histogram cdf at the ith breakpoint, and Y''_i is the approximate second derivative at the ith breakpoint. The values for Y'_i and Y''_i are computed using the following 3-point derivatives:

$$
Y'_i = \frac{Y_{i+1} - Y_{i-1}}{b_{i+1} - b_{i-1}} \qquad (3.30)
$$

and

$$
Y''_i = \frac{Y'_{i+1} - Y'_{i-1}}{b_{i+1} - b_{i-1}} . \qquad (3.31)
$$

Note that in Eq. (3.30) and Eq. (3.31), the expressions for Y'_0, Y'_K, Y''_0 and Y''_K require knowledge of b_{-2}, b_{-1}, b_{K+1}, b_{K+2}, Y_{-2}, Y_{-1}, Y_{K+1}, and Y_{K+2}. The choice of these additional values may have a significant impact on the resulting CPA estimate [7]. Alternatively, 2-point derivatives may be used at the endpoints to eliminate the need to choose additional endpoint values. In any event, once the coefficients $\{a_{ij}\}$ are computed, the resulting CPA estimate of the memoryless LO nonlinearity is

$$
\hat{g}(\rho) = - \sum_{i=0}^{K-1} \frac{2a_{i2} + 6a_{i3}\rho + 12a_{i4}\rho^2 + 20a_{i5}\rho^3}{a_{i1} + 2a_{i2}\rho + 3a_{i3}\rho^2 + 4a_{i4}\rho^3 + 5a_{i5}\rho^4} I_{[b_i, b_{i+1})}(\rho) + \frac{1}{\rho} . \qquad (3.32)
$$

The CPALT algorithm is similar to the basic CPA method except that a linear transformation is performed on each bin of the histogram cdf. The strength of the linear transformation is that it greatly reduces the complexity

of the equations used to compute the CPA coefficients. In particular, the linear transformation is given by the pair of equations [7]: $\tilde{\eta}_i \doteq \eta - b_i$, and $\Delta b_i \doteq b_{i+1} - b_i$. This transformation shifts each interval to the origin. The resulting CPALT estimate of the noise cdf is

$$\hat{F}_n(\eta) = \sum_{i=0}^{K-1} \tilde{y}_i(\tilde{\eta}_i) I_{[0, \Delta b_i)}(\tilde{\eta}_i), \quad \tilde{\eta}_i = \eta - b_i \qquad (3.33)$$

where the polynomial curve for each interval is

$$\tilde{y}_i(\tilde{\eta}_i) = \alpha_{i0} + \alpha_{i1}\tilde{\eta}_i + \alpha_{i2}\tilde{\eta}_i^2 + \cdots + \alpha_{i5}\tilde{\eta}_i^p \qquad (3.34)$$

and $\{\alpha_{ij}\}$ are the transformed polynomial coefficients. The resulting transformed coefficients for $p = 5$ are computed via

$$\begin{bmatrix} 1 & \Delta b_i & \Delta b_i^2 & \Delta b_i^3 & \Delta b_i^4 & \Delta b_i^5 \\ 1 & 0 & 0 & 0 & 0 & 0 \\ 0 & 1 & 2\Delta b_i & 3\Delta b_i^2 & 4\Delta b_i^3 & 5\Delta b_i^4 \\ 0 & 1 & 0 & 0 & 0 & 0 \\ 0 & 0 & 2 & 6\Delta b_i & 12\Delta b_i^2 & 20\Delta b_i^3 \\ 0 & 0 & 2 & 0 & 0 & 0 \end{bmatrix} \begin{bmatrix} \alpha_{i0} \\ \alpha_{i1} \\ \alpha_{i2} \\ \alpha_{i3} \\ \alpha_{i4} \\ \alpha_{i5} \end{bmatrix} = \begin{bmatrix} Y_{i+1} \\ Y_i \\ Y_{i+1}' \\ Y_i' \\ Y_{i+1}'' \\ Y_i'' \end{bmatrix}. \qquad (3.35)$$

By inspection, $\alpha_{i0} = Y_i$, $\alpha_{i1} = Y_i'$, and $\alpha_{i2} = Y_i''/2$. Thus, Eq. (3.35) can be reduced to a system of three equations in three unknowns, resulting in a decrease in implementation complexity. Once the coefficients $\{\alpha_{ij}\}$ are computed, the CPALT estimate of the memoryless LO nonlinearity is given by

$$\hat{g}(\rho) = -\sum_{i=0}^{K-1} \frac{2\alpha_{i2} + 6\alpha_{i3}\tilde{\rho}_i + 12\alpha_{i4}\tilde{\rho}_i^2 + 20\alpha_{i5}\tilde{\rho}_i^3}{\alpha_{i1} + 2\alpha_{i2}\tilde{\rho}_i + 3\alpha_{i3}\tilde{\rho}_i^2 + 4\alpha_{i4}\tilde{\rho}_i^3 + 5\alpha_{i5}\tilde{\rho}_i^4} I_{[0, \Delta b_i)}(\tilde{\rho}_i) + \frac{1}{\rho}, \quad (3.36)$$

where $\tilde{\rho}_i = \rho - b_i$.

The CPALT algorithm may be further simplified by invoking the following argument. Recall that a function with discontinuities will also have discontinuous derivatives. Such a function is usually an unacceptable estimate for most continuous pdfs of interest. However, the CPALT algorithm (as well as the other CPA algorithms) utilizes the 3-point derivatives given by Eq. (3.30) and Eq. (3.31) to compute the estimated deriavtives at the

27

breakpoints. Thus, an auxiliary function can be used in place of the initial cdf estimate, $\hat{F}_n(\eta)$, and it need not be continuous at the breakpoints. However, the auxiliary function must satisfy the constraint that its component first and second derivatives be equal at the breakpoints. The result is the CPA with auxiliary function method of estimating the noise pdf and corresponding LO nonlinearity. Formally, let $H(\eta)$ be the auxiliary function, where

$$H(\eta) = \sum_{i=0}^{K-1} \bar{y}_i(\tilde{\eta}_i) I_{[0,\Delta b_i)}(\tilde{\eta}_i), \quad \tilde{\eta}_i = \eta - b_i \qquad (3.37)$$

and

$$\bar{y}_i(\tilde{\eta}_i) = \beta_{i1}\tilde{\eta}_i + \beta_{i2}\tilde{\eta}_i^2 + \beta_{i3}\tilde{\eta}_i^3 + \beta_{i4}\tilde{\eta}_i^4. \qquad (3.38)$$

The approximation order is $p = 4$ and is determined by the constraints on $H(\eta)$, namely

$$
\begin{aligned}
\bar{y}_i'(\tilde{\eta}_i)|_{\tilde{\eta}_i=\Delta b_i} &= \bar{y}_{i+1}'(\tilde{\eta}_i)|_{\tilde{\eta}_i=\Delta b_i} &= Y_i' \\
\bar{y}_i'(\tilde{\eta}_i)|_{\tilde{\eta}_i=0} &= \bar{y}_{i-1}'(\tilde{\eta}_i)|_{\tilde{\eta}_i=0} &= Y_{i-1}' \\
\bar{y}_i''(\tilde{\eta}_i)|_{\tilde{\eta}_i=\Delta b_i} &= \bar{y}_{i+1}''(\tilde{\eta}_i)|_{\tilde{\eta}_i=\Delta b_i} &= Y_i'' \\
\bar{y}_i''(\tilde{\eta}_i)|_{\tilde{\eta}_i=0} &= \bar{y}_{i-1}'(\tilde{\eta}_i)|_{\tilde{\eta}_i=0} &= Y_{i-1}''.
\end{aligned}
\qquad (3.39)
$$

The coefficients $\{\beta_{ij}\}$, $i = 0, \ldots, K-1$ and $j = 1, \ldots, 4$, are given by

$$
\begin{bmatrix}
1 & 2\Delta b_i & 3\Delta b_i & 4\Delta b_i \\
1 & 0 & 0 & 0 \\
0 & 2 & 6\Delta b_i & 12\Delta b_i \\
0 & 2 & 0 & 0
\end{bmatrix}
\begin{bmatrix}
\beta_{i1} \\
\beta_{i2} \\
\beta_{i3} \\
\beta_{i4}
\end{bmatrix}
\begin{bmatrix}
Y_i' \\
Y_{i-1}' \\
Y_i'' \\
Y_{i-1}''
\end{bmatrix}
\qquad (3.40)
$$

or,

$$
\begin{bmatrix} \beta_{i1} \\ \beta_{i2} \\ \beta_{i3} \\ \beta_{i4} \end{bmatrix} = \begin{bmatrix} Y'_{i-1} \\ \dfrac{Y''_{i-1}}{2} \\ \dfrac{-\Delta b_i(Y''_i + 2Y''_{i-1}) + 3(Y'_i - Y'_{i-1})}{2\Delta b_i^2} \\ \dfrac{\Delta b_i(Y''_i + Y''_{i-1}) - 2(Y'_i - Y'_{i-1})}{4\Delta b_i^3} \end{bmatrix} . \tag{3.41}
$$

The resulting CPA with auxiliary function estimate of the memoryless LO nonlinearity is

$$
\hat{g}(\rho) = -\sum_{i=0}^{K-1} \frac{2\beta_{i2} + 6\beta_{i3}\tilde{\rho}_i + 12\beta_{i4}\tilde{\rho}_i^2}{\beta_{i1} + 2\beta_{i2}\tilde{\rho}_i + 3\beta_{i3}\tilde{\rho}_i^2 + 4\beta_{i4}\tilde{\rho}_i^3} I_{[0,\Delta b_i)}(\tilde{\rho}_i) + \frac{1}{\rho}, \quad \tilde{\rho}_i = \rho - b_i. \tag{3.42}
$$

The CPAGT algorithm is particularly useful in environments where Gaussian noise is present. Since the noise observations that correspond to the tails of the pdf occur infrequently, it is difficult to estimate these regions nonparametrically. However, if a Gaussian-like tail structure is assumed, it is necessary to estimate only the mean and variance, since these two parameters completely characterize the Gaussian pdf. This approach is the foundation of the CPAGT algorithm. Beginning with a histogram approximation of the pdf (not the cdf as in the basic CPA and CPALT methods), the CPAGT estimate, $\hat{f}_n(\eta)$, of the noise pdf, $f_n(\eta)$ is

$$
\hat{f}_n(\eta) = \sum_{i=0}^{K-1} y_i(\eta) I_{[b_i, b_{i+1})}(\eta) \tag{3.43}
$$

where, in this case, $p = 3$ and

$$
y_i(\eta) = a_{i0} + a_{i1}\eta + a_{i2}\eta^2 + a_{i3}\eta^3. \tag{3.44}
$$

The CPA coefficients $a_{ij}, i = 1, 2, \ldots, K-2$ and $j = 0, 1, \ldots, p$, for $p = 3$ are given by [7]

$$
\begin{bmatrix} 1 & b_{i+1} & b_{i+1}^2 & b_{i+1}^3 \\ 1 & b_i & b_i^2 & b_i^3 \\ 0 & 1 & 2b_{i+1} & 3b_{i+1}^2 \\ 0 & 1 & 2b_i & 3b_i^2 \end{bmatrix} \begin{bmatrix} a_{i0} \\ a_{i1} \\ a_{i2} \\ a_{i3} \end{bmatrix} = \begin{bmatrix} Y_{i+1} \\ Y_i \\ Y'_{i+1} \\ Y'_i \end{bmatrix} . \tag{3.45}
$$

29

However, the first ($b_0 \leq \eta < b_1$) and last ($b_{K-1} \leq \eta < b_K$) bins of the histogram pdf are approximated by the Gaussian pdf

$$f_g(\eta) = \frac{1}{\sqrt{2\pi\hat{\sigma}^2}} e^{\frac{-(\eta-\hat{\mu})^2}{2\hat{\sigma}^2}} \tag{3.46}$$

where

$$\hat{\mu} = \frac{1}{Q} \sum_{k=1}^{Q} \eta_k \tag{3.47}$$

and

$$\hat{\sigma}^2 = \frac{1}{Q-1} \sum_{k=1}^{Q} (\eta_k - \hat{\mu})^2. \tag{3.48}$$

To achieve the required continuity at the breakpoints, the values of Y_1, Y_1', Y_{K-1}, and Y_{K-1}' are computed from $f_g(\eta)$. The resulting CPAGT estimate of the memoryless LO nonlinearity is

$$\hat{g}(\rho) = \begin{cases} -\sum_{i=1}^{K-2} \frac{a_{i1}+2a_{i2}\rho+2a_{i3}\rho^2}{a_{i0}+a_{i1}\rho+a_{i2}\rho^2+a_{i3}\rho^3} I_{[b_i,b_{i+1})}(\rho) + \frac{1}{\rho}, & b_1 \leq \rho < b_{K-1} \\[2em] \frac{\rho-\hat{\mu}}{\hat{\sigma}^2}, & \begin{array}{l} b_0 \leq \rho < b_1 \text{ or} \\ b_{K-1} \leq \rho < b_K \end{array} \end{cases} \tag{3.49}$$

Note that a linear transformation may be used in conjunction with this method to reduce the complexity of Eq. (3.45).

3.4   The FSA Algorithm

This section presents an algorithm for estimating pdfs that is based on the Fourier series ([13], Ch. 8). Its major features are that: (1) the approximation is continuous throughout its domain; (2) it possesses an arbitrary number of continuous derivatives; and (3) no quantization process is required, i.e., each data sample contributes uniquely to the overall estimate.

Given the set of Q observed noise magnitude samples $\{\eta_i\}$ with minimum value η_{min} and maximum value η_{max}, the *Fourier series approximation* (FSA) of the noise magnitude pdf, denoted $\hat{f}_n(\eta)$, is given by the following

expression:

$$
\hat{f}_n(\eta) = \begin{cases} \frac{a_0}{2} + \sum_{k=1}^{p} \{a_k \cos(k\omega_0\eta) + b_k \sin(k\omega_0\eta)\} \\ \qquad\qquad \text{for } \eta_{\min} \leq \eta \leq \eta_{\max} \\ 0 \qquad\qquad\qquad\qquad \text{otherwise .} \end{cases} \qquad (3.50)
$$

The natural frequency of the FSA is given by $\omega_0 = 2\pi/T$ where $T = \eta_{max} - \eta_{min}$ is the "period." The coefficients $\{a_k\}$ and $\{b_k\}$ are determined by minimizing the ISE between $\hat{f}_n(\eta)$ and $f_n(\eta)$, the actual noise magnitude pdf. This expression is written as

$$
\begin{aligned}
ISE &= \int_{\eta_{\min}}^{\eta_{\max}} [\hat{f}_n(\eta) - f_n(\eta)]^2 d\eta \\
&= \int_{\eta_{\min}}^{\eta_{\max}} \left[f_n(\eta) - \frac{a_0}{2} - \sum_{k=1}^{p} a_k \cos(k\omega_0\eta) \right. \\
&\qquad\qquad \left. - \sum_{k=1}^{p} b_k \sin(k\omega_0\eta) \right]^2 d\eta .
\end{aligned} \qquad (3.51)
$$

Differentiating Eq. (3.51) with respect to a_0, a_k, and b_k, equating each expression to zero, and noting that the integration of the sine or cosine functions over an integer multiple of its period is equal to zero and that $\int_{\eta_{\min}}^{\eta_{\max}} f_n(\eta)\, d\eta = 1$,[2] yields the following results:

$$
a_0 = \frac{2}{\eta_{\max} - \eta_{\min}}, \qquad (3.52)
$$

$$
a_k = \frac{2}{\eta_{\max} - \eta_{\min}} \int_{\eta_{\min}}^{\eta_{\max}} \cos(k\omega_0\eta) f_n(\eta) d\eta, \; k = 1,\ldots,p, \qquad (3.53)
$$

and

$$
b_k = \frac{2}{\eta_{\max} - \eta_{\min}} \int_{\eta_{\min}}^{\eta_{\max}} \sin(k\omega_0\eta) f_n(\eta) d\eta, \; k = 1,\ldots,p. \qquad (3.54)
$$

---

[2]It is assumed that the support length of the actual pdf $f_n(\eta)$ is $\eta_{max} - \eta_{min}$. However, this is not a necessary constraint, since truncation can be used to approximate a pdf with infinite support.

Recalling that the expectation of a function $h(X)$ of the random variable X is given by $E\{h(X)\} = \int_x h(x)\,f_X(x)\,dx$, Eq. (3.53) and Eq. (3.54) can be written as

$$
\begin{aligned}
a_k &= \frac{2}{\eta_{\max} - \eta_{\min}} E\{\cos(\omega_0\,k\,n)\}, \quad k = 1,\dots,p \\[2mm]
b_k &= \frac{2}{\eta_{\max} - \eta_{\min}} E\{\sin(\omega_0\,k\,n)\}, \quad k = 1,\dots,p.
\end{aligned}
\tag{3.55}
$$

Since the actual pdf of n is unavailable in many applications, Eq. (3.55) can be approximated using the sample averages, resulting in the estimated FSA coefficients:

$$
\hat{a}_0 = a_0 = \frac{2}{\eta_{\max} - \eta_{\min}}
\tag{3.56}
$$

$$
\hat{a}_k = \frac{2}{\eta_{\max} - \eta_{\min}} \frac{1}{Q} \sum_{i=1}^{Q} \cos(k\,\omega_0\,\eta_i), \qquad k = 1,\dots,p
$$

$$
\hat{b}_k = \frac{2}{\eta_{\max} - \eta_{\min}} \frac{1}{Q} \sum_{i=1}^{Q} \sin(k\,\omega_0\,\eta_i), \qquad k = 1,\dots,p.
$$

Another method of approximating the FSA coefficients is discussed in [5] and involves first estimating $f_n(\eta)$ via a histogram and then using the result in Eq. (3.53) and Eq. (3.54). If the value of the histogram at the ith breakpoint, b_i, is Y_i, and K is the number of histogram bins, then the FSA coefficients can be estimated by

$$
\hat{a}_0 = a_0 = \frac{2}{\eta_{\max} - \eta_{\min}}
\tag{3.57}
$$

$$
\hat{a}_k = \frac{2}{\eta_{\max} - \eta_{\min}} \sum_{i=0}^{K-1} Y_i(b_{i+1} - b_i) \cos(k\,\omega_0\,b_i), \qquad k = 1,\dots,p
$$

$$
\hat{b}_k = \frac{2}{\eta_{\max} - \eta_{\min}} \sum_{i=0}^{K-1} Y_i(b_{i+1} - b_i) \sin(k\,\omega_0\,b_i), \qquad k = 1,\dots,p.
$$

To implement the memoryless LO nonlinearity, Eq. (3.50) and Eq. (3.56) are used directly in the expression for $g(\rho_i)$ given in Eq. (2.16). The resulting estimate of $g(\rho_i)$ is

$$
\hat{g}(\rho_i) = \frac{\sum_{k=1}^{p} \hat{a}_k k\omega_0 \sin(k\omega_0\rho_i) - \sum_{k=1}^{p} \hat{b}_k k\omega_0 \cos(k\omega_0\rho_i)}{\frac{a_0}{2} + \sum_{k=1}^{p} \hat{a}_k \cos(k\omega_0\rho_i) + \sum_{k=1}^{p} \hat{b}_k \sin(k\omega_0\rho_i)} + \frac{1}{\rho_i}
\tag{3.58}
$$

for $\eta_{min} \le \rho_i \le \eta_{max}$ and 0 otherwise.

The major features of the FSA algorithm can be seen from Eq. (3.50) and Eq. (3.56). First, since the FSA estimate of a pdf is a sum of continuous functions the overall result is a continuous function. Second, since the sine and cosine functions are infinitely differentiable, the resulting pdf estimate is also. Finally, each data sample contributes uniquely (no quantization) to the FSA estimate through Eq. (3.56).

3.5 The Kernel Algorithm

Kernel pdf estimators have received considerable interest in the past few decades ([14], Ch. 6 and references). Like the histogram, the kernel estimator is a nonparametric method, i.e., it does not assume that the pdf being estimated has a particular form. Instead, the resulting shape of the pdf estimate is solely a function of the observed data samples. The kernel estimator also has a number of advantages over the histogram: (1) it is continuous, (2) it may possess continuous derivatives, (3) it requires, on average, less samples to form an estimate than does the histogram, and (4) it is readily applicable to the estimation of multivariate pdfs and their gradients. Its major disadvantage is that in many cases the kernel estimator requires considerably more computation than does the histogram. However, with the availability of specialized processors, this increased computational burden is probably not an issue.

Since the subject of kernel estimation is such a rich area, the remainder of this section provides a brief overview of the topic. In particular, the kernel estimators for univariate and multivariate pdfs will be presented, with emphasis placed on their application to LO detection.

Let $\{\eta_i\}$ be the set of Q observed samples of the noise magnitude random variable n. The kernel estimator of $f_n(\eta)$, the pdf of n, may be written as

$$\hat{f}_n(\eta) = \frac{1}{Q h} \sum_{i=1}^{Q} K\left(\frac{\eta - \eta_i}{h}\right). \tag{3.59}$$

The kernel window, $K(t)$, determines the weighting effect that the samples $\{\eta_i\}$ have on the pdf estimate at the value η. The variable h is known as the "smoothing parameter" and determines the range of samples $\{\eta_i\}$ that will affect the pdf estimate at the value η.

33

Recall that the memoryless LO nonlinearity requires the first derivative of $f_n(\eta)$. Using the kernel estimator, this can be approximated as

$$\frac{d}{d\eta}\hat{f}_n(\eta) = \frac{d}{d\eta}\left[\frac{1}{Qh}\sum_{i=1}^{Q}K\left(\frac{\eta - \eta_i}{h}\right)\right] = \frac{1}{Qh^2}\sum_{i=1}^{Q}K'\left(\frac{\eta - \eta_i}{h}\right). \quad (3.60)$$

As can be seen, the kernel estimator can provide a direct approximation of $f_n'(\eta)$, which relieves the need to use numerical differentiation (as in the histogram method).

The characteristics of the kernel pdf estimator of Eq. (3.59) are primarily determined by the kernel and the smoothing parameter. Kernels usually satisfy the following constraints:

$$\begin{array}{rcl} K(t) & \geq & 0 \\ \int K(t)\,dt & = & 1 \\ \int t\,K(t)\,dt & = & 0. \end{array} \quad (3.61)$$

Two kernels which are widely used are (1) the Epanechnikov kernel, given by

$$K(t) = \frac{3}{4}(1 - t^2)\,I_{(-1,1)}(t), \quad (3.62)$$

and (2) the Gaussian kernel, given by

$$K(t) = \frac{1}{\sqrt{2\pi}}\,e^{-t^2/2}. \quad (3.63)$$

The Epanechnikov kernel is particularly useful since it minimizes the *asymptotic mean ISE* (AMISE) between $f_n(\eta)$ and $\hat{f}_n(\eta)$. Recalling the definition of ISE, e.g, Eq. (3.11) or Eq. (3.51), the *mean ISE* (MISE) is given by

$$MISE\,[\hat{f}_n(\eta)] \doteq E\left\{ISE\,[\hat{f}_n(\eta)]\right\}, \quad (3.64)$$

and the AMISE is defined to be the main terms of the Taylor series approximation of the MISE ([14], Ch. 2). The Gaussian kernel, on the other hand, is particularly useful in situations when higher-order derivatives of $\hat{f}_n(\eta)$ are required.[3]

_____

[3]For an extensive list of kernel functions see reference [14], Chapter 6.

The smoothing parameter h also affects the AMISE of $\hat{f}_n(\eta)$. A useful result shown in ([14], Ch. 6) is that for Gaussian data $\{\eta_i\}$ and a Gaussian kernel, the value of h which minimizes the AMISE is

$$h = \left(\frac{4}{3}\right)^{1/5} \sigma Q^{-1/5} \tag{3.65}$$

where σ^2 is the variance of n. Equation (3.65) can be a useful starting point for determining a value of h suitable for the given application. In most cases, the value of h will need to be decreased as the data becomes "less Gaussian."

The simplest way to apply the univariate kernel estimator to LO detection is by direct substitution into the memoryless LO nonlinearity, $g(\rho_i)$, of Eq. (2.16). Thus, the kernel estimate of $g(\rho_i)$ is

$$\hat{g}(\rho_i) = -\frac{\hat{f}'_n(\rho_i)}{\hat{f}_n(\rho_i)} + \frac{1}{\rho_i} = -\frac{1}{h}\frac{\sum_{i=1}^{Q} K'\left(\frac{\rho_i - \eta_i}{h}\right)}{\sum_{i=1}^{Q} K\left(\frac{\rho_i - \eta_i}{h}\right)} + \frac{1}{\rho_i}. \tag{3.66}$$

More sophisticated forms of $\hat{g}(\rho_i)$ can be derived if characteristics concerning the noise magnitude pdf are known prior to detector implementation.

3.6 Simulation Results and Comparison of Techniques

This section presents the simulation results for the memoryless LO detector implementations discussed in Sections 3.1 through 3.5. Results are presented for LO detection in both a standard QPSK system, Eq. (2.15) and Eq. (2.16), and a QPSK DSSS system, Eq. (2.24). In implementing the LO nonlinearities, the following *critical* assumption is made: since the environments of interest exhibit high *jammer-to-signal* (J/S) ratios, *the received signal magnitude, r, is approximately equal to the noise magnitude, n, and thus $f_r(\cdot) \approx f_n(\cdot)$*. In other words, the received magnitude pdf was used in place of the noise magnitude pdf in the implementation of the memoryless LO nonlinearities. Since the histogram, MIPA, and histogram FSA methods were examined in [5], the focus of this section is primarily on the various CPA

algorithms and the FSA method described by Eq. (3.56). Also, analysis of the kernel algorithm is postponed until Section 4.3.

The first scenario examined was the *probability of bit error* (P_b) performance of the various LO nonlinearity implementation algorithms in a standard QPSK system subjected to a single *continuous wave* (CW) jammer. The goal of analyzing these algorithms in a QPSK system is to determine parameter settings to be used in the QPSK DSSS system. Figure 3.1 through Fig. 3.3 illustrates P_b for the CPALT, CPA with auxiliary function, and CPAGT methods for various values of f_j/R_s, the ratio of the jammer's frequency to the information signal's symbol rate, and N, the number of samples per symbol, i.e., the length of the signal vectors.[4] The value of J/S was fixed at 30 dB and the system parameters are shown in Table 3.1. As can be seen from the graphs, all three methods exhibit the same performance characteristics: (1) P_b decreases as f_j/R_s increases, and (2) for a given f_j/R_s, P_b remains relatively constant once N is sufficiently large, approximately $N \geq 20$.

System Parameters for the QPSK System		
	Parameter Name	Parameter Value
Transmitter and Receiver Parameters	Sampling frequency (in Hz)	1
	Samples per symbol (N)	5 to 50 by 5
	Number of CPA bins (K)	10
	Number of samples per CPA (Q)	50,400
Channel Parameters	J/S (in dB)	30
	f_j/R_s	0.00496 to 0.496 by 0.098208
	E_b/N_0 (in dB)	10
	Symbols used for P_b calculation	1,008

Table 3.1: System parameters for the CPA algorithms in a QPSK system: examination of P_b relative to N and f_j/R_s.

Next, the effects of K, the number of bins, and Q, the number of available samples used in the approximation (i.e., the number of received magnitude samples), on P_b was examined for the system parameters in Table 3.2 and

---

[4]The results shown in the these figures were compiled from only a single simulation run. Thus, these graphs should be used for the purpose of determining performance trends, and not quantitative values of P_b.
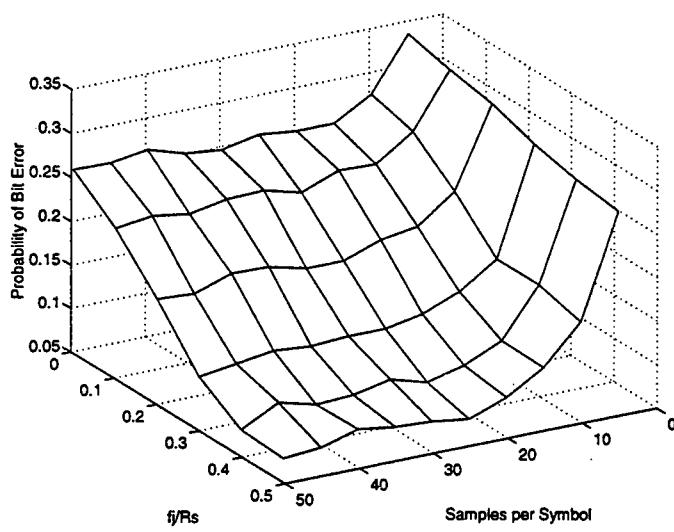
Figure 3.1: Probability of bit error (1 CW jammer at J/S=30 dB) for the LO QPSK simulation - CPA with linear transform implementation
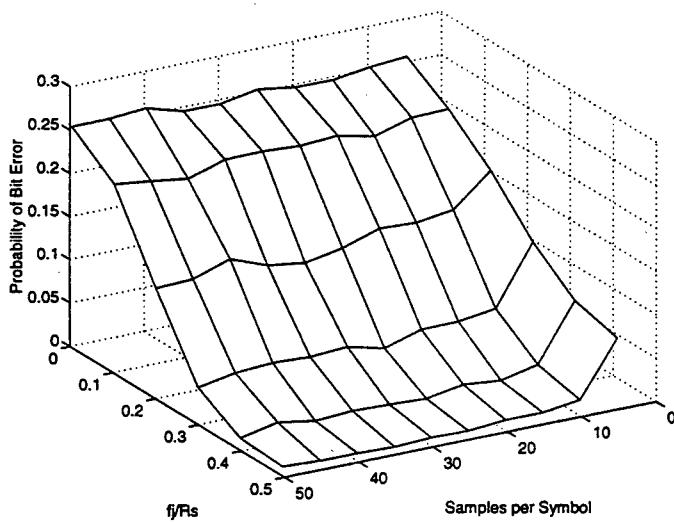
Figure 3.2: Probability of bit error (1 CW jammer at J/S=30 dB) for the LO QPSK simulation - CPA with auxiliary function implementation

37
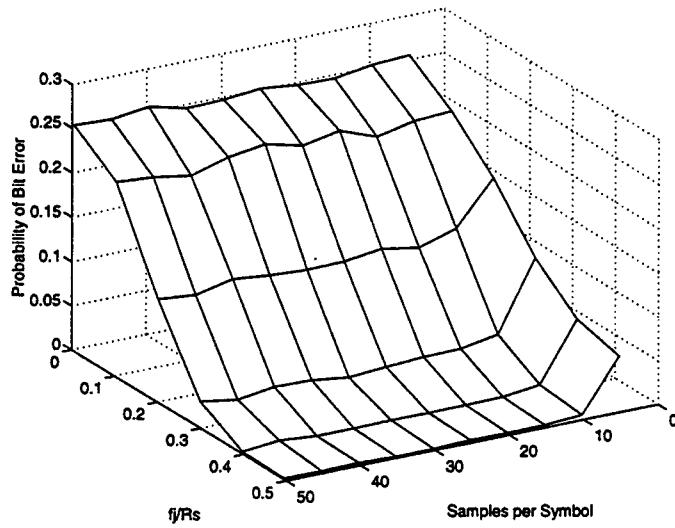
Figure 3.3: Probability of bit error (1 CW jammer at J/S=30 dB) for the LO QPSK simulation - CPA with Gaussian tails implementation

$J/S = 30dB$, with $f_j/R_s = 0.496$.[5] The P_b plot for the CPALT algorithm, Fig. 3.4, indicates that there is a steady decrease in P_b as both K and Q are increased. The CPA with auxiliary function, Fig. 3.5, also exhibits a decrease in P_b as K is increased, but is less sensitive to varying Q. Finally, the CPAGT algorithm, Fig. 3.6, has relatively uniform performance for all K and Q examined (provided Q is sufficiently large for the given K).

Finally, the P_b performance of the various CPA algorithms was examined for various J/S and K values. The results corresponding to $f_j/R_s = 0.496$ and the system parameters in Table 3.3 are shown in Fig. 3.7 to Fig. 3.9.[6] The P_b plots indicate that all the methods have relatively low P_b in the region $20dB \leq J/S \leq 50dB$, provided K is sufficiently large, and also in the region $J/S \approx -10dB$. However, in the intermediate region of $-10dB < J/S < 10dB$, P_b is relatively large. While the reason for this increase in

---

[5]The results shown in the these figures were compiled from only a single simulation run. Thus, these graphs should be used for the purpose of determining performance trends, and not quantitative values of P_b.

[6]The results shown in the these figures were compiled from an average of three simulation runs.

System Parameters for the QPSK System		
	Parameter Name	Parameter Value
Transmitter	Sampling frequency (in Hz)	1
and	Samples per symbol (N)	25
Receiver	Number of CPA bins (K)	4 to 20 by 2
Parameters	Number of samples per CPA (Q)	5,000 to 50,000 by 5,000
Channel	J/S (in dB)	30
Parameters	f_j/R_s	0.496
	E_b/N_0 (in dB)	10
	Symbols used for P_b calculation	10,000

Table 3.2: System parameters for the CPA algorithms in a QPSK system: examination of P_b relative to K and Q.
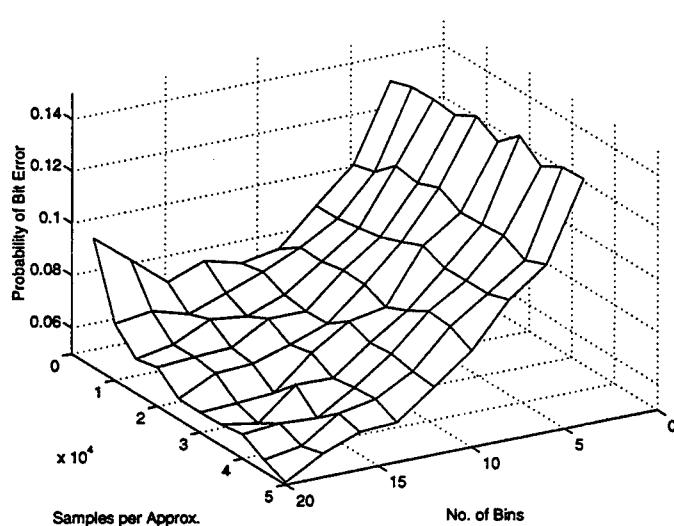
Figure 3.4: Probability of bit error (1 CW jammer at J/S=30 dB) for the LO QPSK simulation - CPA with linear transform implementation
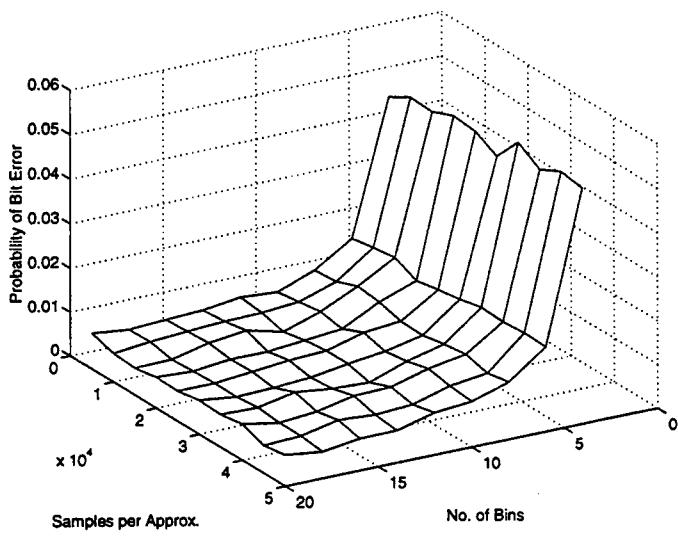
Figure 3.5: Probability of bit error (1 CW jammer at J/S=30 dB) for the LO QPSK simulation - CPA with auxiliary function implementation
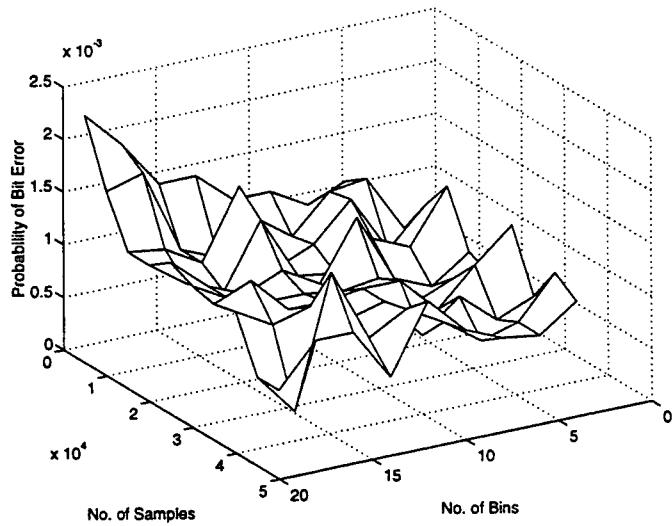

Figure 3.6: Probability of bit error (1 CW jammer at J/S=30 dB) for the LO QPSK simulation - CPA with Gaussian tails implementation

P_b is not fully known, one possible explanation is that under the large J/S assumption that $f_r(\cdot) \approx f_n(\cdot)$, the LO nonlinearity attempts to mitigate the dominant component of the interference. For $20dB \leq J/S \leq 50dB$, the CW jammer dominates, while for $J/S \approx -10dB$ the Gaussian background noise is dominant. In both these situations the LO nonlinearity is able to mitigate the dominant interference, and the effects of the other interferer are minimal. However, for $-10dB < J/S < 10dB$, neither interferer is dominant, so the nonlinearity must attempt to mitigate both, with a resulting increase in P_b. A further investigation must be performed before the exact cause behind this P_b performance characteristic can be determined.

System Parameters for the QPSK System		
	Parameter Name	Parameter Value
Transmitter and Receiver Parameters	Sampling frequency (in Hz)	1
	Samples per symbol (N)	25
	Number of CPA bins (K)	4 to 20 by 2
	Number of samples per CPA (Q)	5,000
Channel Parameters	J/S (in dB)	-10 to 50 by 10
	f_j/R_s	0.496
	E_b/N_0 (in dB)	10
	Symbols used for P_b calculation	1,000

Table 3.3: System parameters for the CPA algorithms in a QPSK system: examination of P_b relative to J/S and K.

The P_b performance of the FSA implementation of the memoryless LO nonlinearity in a QPSK system was also examined. For a single CW jammer with $J/S = 30dB$, the P_b relative to f_j/R_s and p, the FSA order, is shown in Fig. 3.10, with the the system parameters given in Table 3.4.[7] As for the CPA algorithms, P_b decreases for the FSA algorithm as f_j/R_s increases. Also, P_b was observed to be lowest in the region $5 \leq p \leq 20$.

With the information garnered in the analysis of the memoryless LO nonlinearities in a QPSK system, a P_b performance analysis of the robust LO nonlinearities in a QPSK DSSS system was then performed. The following nonlinearity parameters were chosen as a result of the preceding analysis.

---

[7]The results shown in the these figures were compiled from an average of three simulation runs.
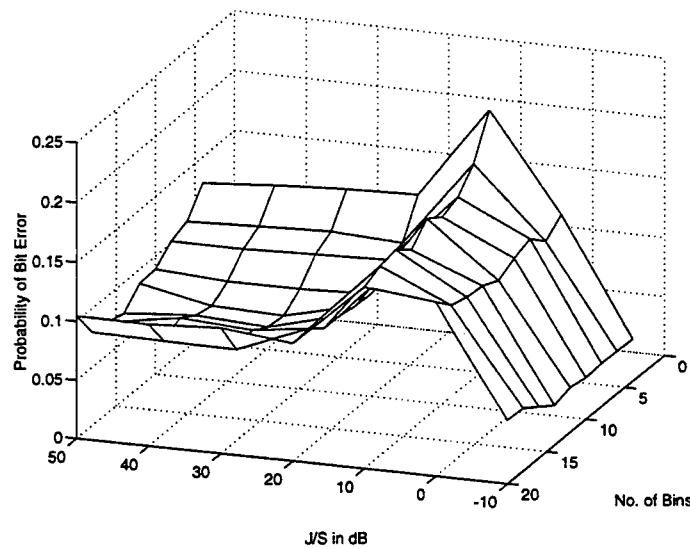
Figure 3.7: Probability of bit error (1 CW jammer) for the LO QPSK simulation - CPA with linear transform implementation
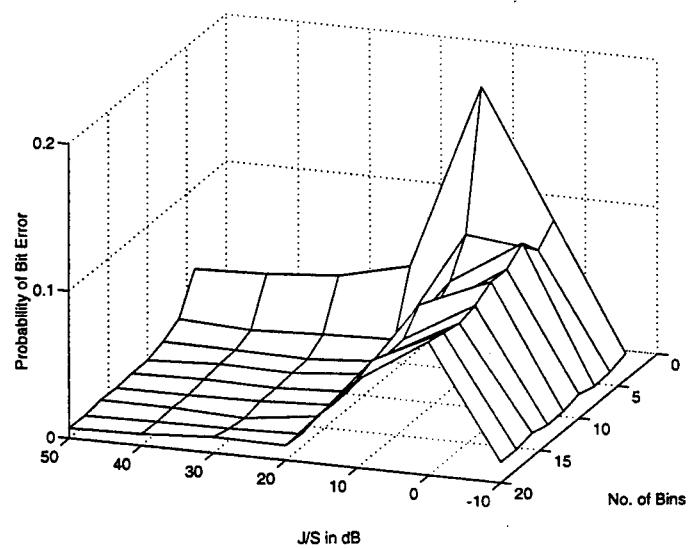
Figure 3.8: Probability of bit error (1 CW jammer) for the LO QPSK simulation - CPA with auxiliary function implementation

42
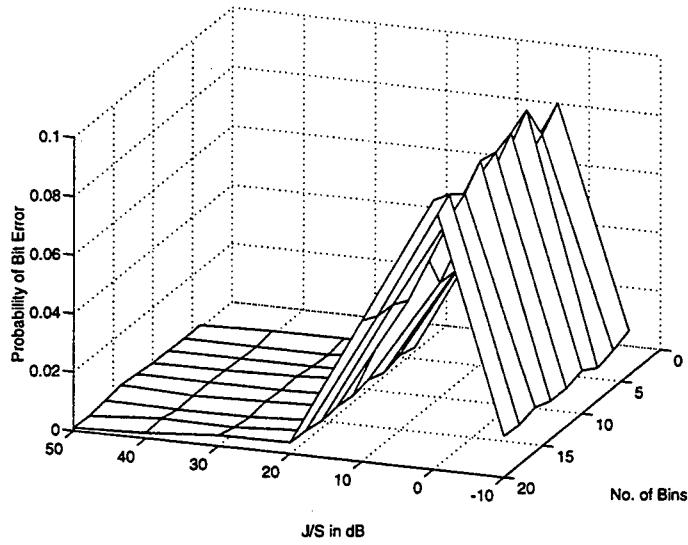
Figure 3.9: Probability of bit error (1 CW jammer) for the LO QPSK simulation - CPA with Gaussian tails implementation

System Parameters for the QPSK System		
	Parameter Name	Parameter Value
Transmitter and Receiver Parameters	Symbol rate (R_s) in Hz	0.05
	Samples per symbol (N)	20
	FSA order (p)	2 to 20 by 2
	Number of samples per FSA (Q)	50,000
Channel Parameters	J/S (in dB)	30
	f_j/R_s	0.00496 to 0.496 by 0.098208
	E_b/N_0 (in dB)	10
	Symbols used for P_b calculation	5,000

Table 3.4: System parameters for the FSA algorithm in a QPSK system: examination of P_b relative to f_j/R_s and p.

43
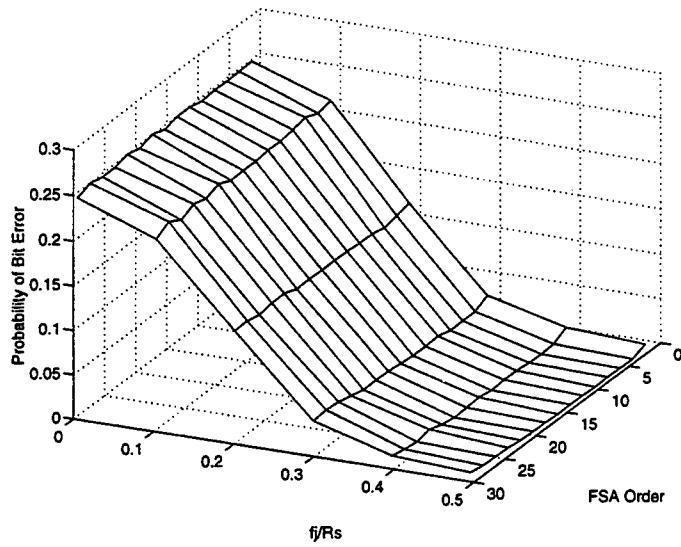
Figure 3.10: Probability of bit error (1 CW jammer) for the LO QPSK simulation - FSA implementation

For the CPA algorithms: $K = 10$ and $Q = 50,400$. For the FSA algorithm: $p = 10$ and 20, and $Q = 50,400$. Using a processing gain $= T/T_c$ of 20 (see Chapter 2), and 2 samples per chip (resulting in $N = 2 \times 20 = 40$), the performance was examined for the various robust LO nonlinearities in a QPSK DSSS system subjected to a single CW jammer with varying J/S and f_j/R_s, with the system parameters provided in Table 3.5.[8] The simulation results for the CPALT, CPA with auxiliary function, and CPAGT algorithms are shown in Fig. 3.11 to Fig. 3.13. Each method exhibited the same P_b characteristic: for sufficiently large J/S ($J/S \geq 10dB$) P_b decreases as f_j/R_s increases. Also, the CPAGT algorithm consistently possessed a P_b lower than the other two CPA methods. The results for the FSA algorithm with $p = 10$ & 20 are shown in Fig. 3.14 and Fig. 3.15. This algorithm also exhibited the performance trend that P_b decreases as f_j/R_s increases. Finally, similar simulation results for the histogram, histogram FSA, and second-order MIPA algorithms, provided from [5], are shown in Fig. 3.16 to

---

[8]The results shown in the the following figures were compiled from an average of three simulation runs.

44

Fig. 3.18 for comparison purposes.

System Parameters for the QPSK DSSS System		
	Parameter Name	Parameter Value
Transmitter and Receiver Parameters	Symbol Rate (R_s) in Hz	0.1
	Chip rate (R_c) in Hz	2
	Samples per chip	2
	Samples per symbol (N)	40
	Number of CPA bins (K)	10
	FSA Order (p)	10 and 20
	Number of samples per CPA and FSA (Q)	50,400
Channel Parameters	J/S (in dB)	0 to 50 by 10
	f_j/R_s	0.00496 to 0.496 by 0.098208
	E_b/N_0 (in dB)	10
	Symbols used for P_b calculation	5,040

Table 3.5: System parameters for the robust memoryless LO nonlinearities in a QPSK DSSS system: examination of P_b relative to J/S and f_j/R_s.

From an examination of all the simulation results, a number of observations can be made. First, while some LO nonlinearity implementation algorithms may exhibit slightly lower P_b than others, in general they all have roughly the same performance characteristics. Second, and probably more importantly, these robust techniques, which use the large J/S assumption that $f_r(\cdot) \approx f_n(\cdot)$, are not as robust as would be desired. In particular, for the case of a single CW jammer, P_b varies greatly as f_j/R_s changes, with low P_b in regions of high f_j/R_s, and *high* P_b in regions of *low* f_j/R_s. Thus, the LO detector performs poorly when the frequency of the CW jammer lies near the center of the transmitted signal's frequency spectrum. The reason(s) behind this poor performance, and a discussion of possible ways to improve it, are the topics of Chapter 5.
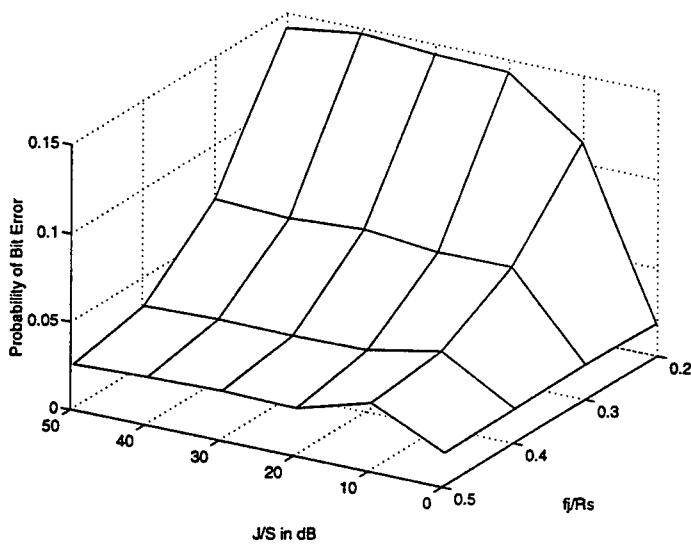
Figure 3.11: Probability of bit error (1 CW jammer) for the LO DSSS simulation - CPA with linear transform implementation
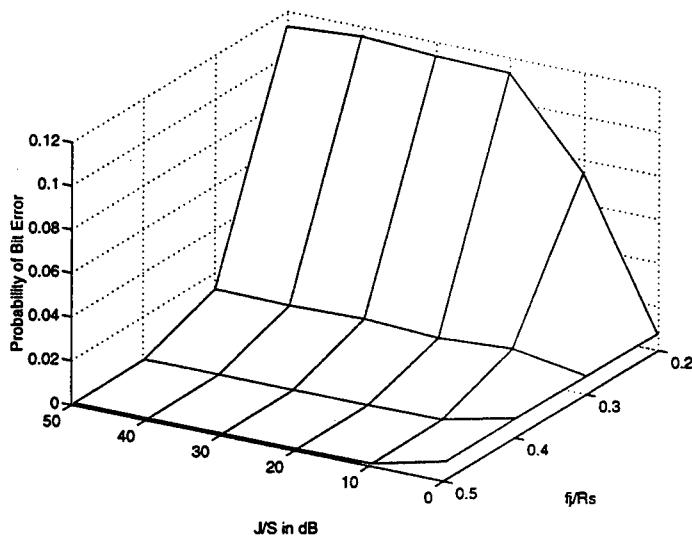
Figure 3.12: Probability of bit error (1 CW jammer) for the LO DSSS simulation - CPA with auxiliary function implementation

46
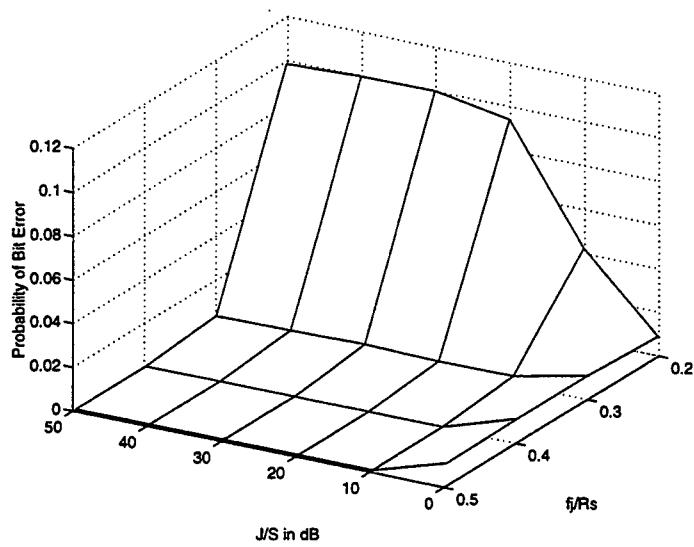
Figure 3.13: Probability of bit error (1 CW jammer) for the LO DSSS simulation - CPA with Gaussian tails implementation
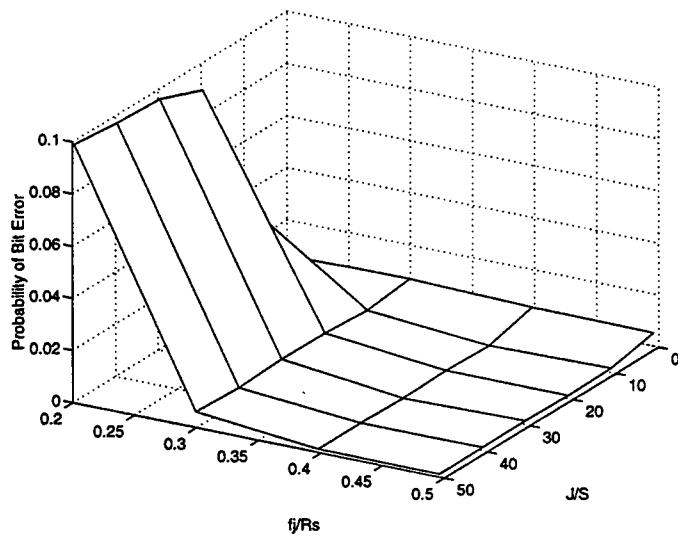
Figure 3.14: Probability of bit error (1 CW jammer) for the LO DSSS simulation - FSA implementation with $p = 10$

47
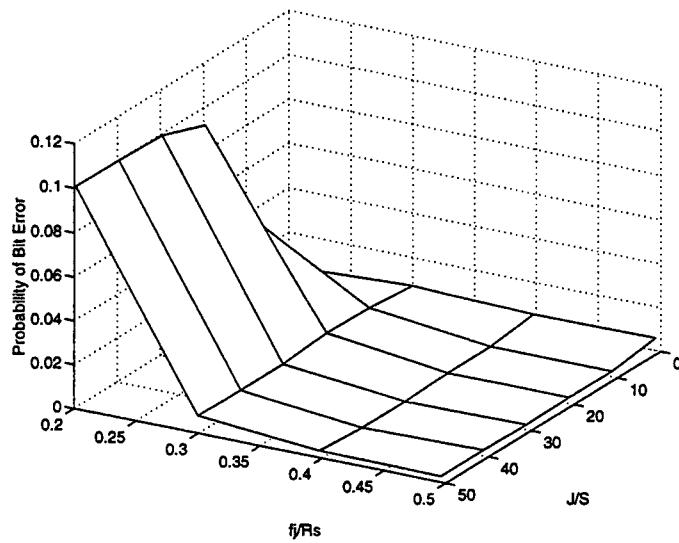
Figure 3.15: Probability of bit error (1 CW jammer) for the LO DSSS simulation - FSA implementation with $p = 20$
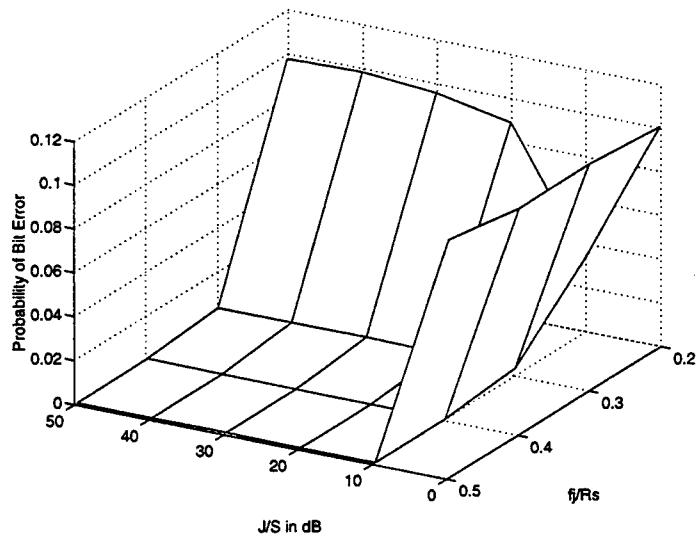

Figure 3.16: Probability of bit error (1 CW jammer) for the LO DSSS simulation - histogram implementation
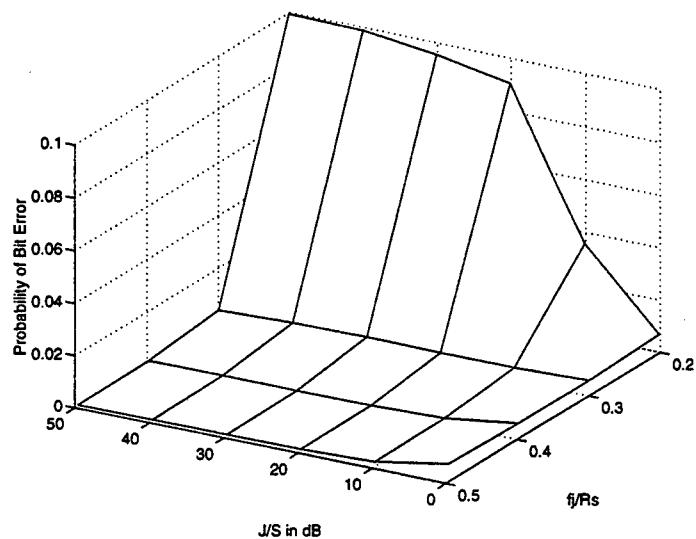
Figure 3.17: Probability of bit error (1 CW jammer) for the LO DSSS simulation - FSA/histogram implementation
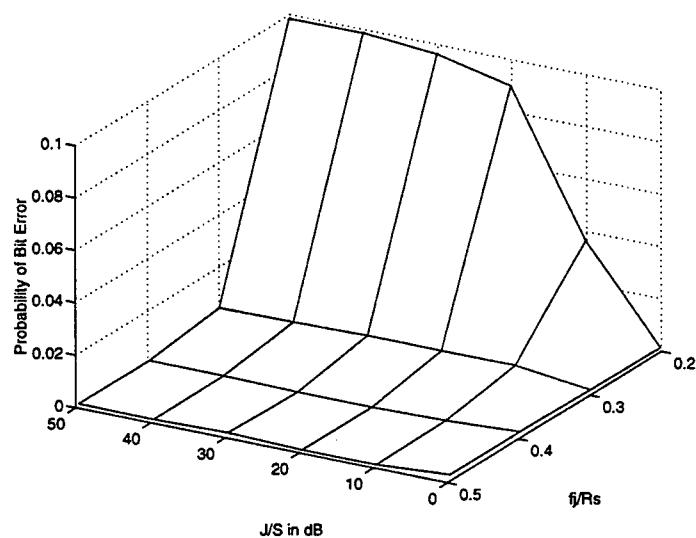
Figure 3.18: Probability of bit error (1 CW jammer) for the LO DSSS simulation - second-order MIPA implementation

3.7 The Direct FSA Implementation of the Memoryless LO Detector

Given a few assumptions, a Fourier series may be used to directly estimate the memoryless LO nonlinearity. Ignoring the $1/\rho$ term, recall that the memoryless LO nonlinearity has the form $g(\rho) = -f_n'(\rho) / f_n(\rho)$. To derive the FSA estimate of $g(\rho)$ the following assumptions are made concerning the noise pdf, $f_n(\eta)$: $f_n(\eta)$ is even symmetric about the origin (and thus has zero mean), and is bounded by η_{max} and η_{min}, where $\eta_{max} = -\eta_{min}$.[9] Begin the derivation by approximating $g(\rho)$ as

$$
\hat{g}(\rho) = \begin{cases} \frac{a_0}{2} + \sum_{k=1}^{P} a_k \cos(k\omega_0\rho) + \sum_{k=1}^{P} b_k \sin(k\omega_0\rho) \\ \qquad\qquad \text{for } \eta_{\min} \leq \rho \leq \eta_{\max} \\ \\ 0 \qquad\qquad\qquad\qquad\qquad \text{otherwise} \end{cases}
\qquad (3.67)
$$

where $T = \eta_{max} - \eta_{min}$ and $\omega_0 = (2\pi)/T$. The coefficients $\{a_k\}$ and $\{b_k\}$ (*which are different from those in Eq. (3.50)*) are chosen so as to minimize the *mean squared error* (MSE) when the observation consists of noise only, i.e., $r = n$. The MSE (denoted by the function J) is given by:

$$
\begin{aligned}
J &= E\left\{[g(r) - \hat{g}(r)]^2\right\}\big|_{r=n} = \int_{-\infty}^{\infty} [g(\rho) - \hat{g}(\rho)]^2 f_n(\rho)\, d\rho \\
\\
&= \int_{\eta_{\min}}^{\eta_{\max}} \left[g(\rho) - \frac{a_0}{2} - \sum_{k=1}^{P} a_k \cos(k\omega_0\rho) - \sum_{k=1}^{P} b_k \sin(k\omega_0\rho)\right]^2 f_n(\rho)\, d\rho\,.
\end{aligned}
\qquad (3.68)
$$

To find a_0 which minimizes J, the expression $\partial J/\partial a_0$ is computed and equated to zero. By symmetry, $\int_{\eta_{\min}}^{\eta_{\max}} \sin(k\omega_0\rho) f_n(\rho)\, d\rho = 0$ and $f_n(\eta_{\min}) = f_n(\eta_{\max})$, resulting in the following equation:

$$
\frac{a_0}{2} + \sum_{k=1}^{P} a_k E[\cos(k\omega_0 n)] = f_n(\eta_{\min}) - f_n(\eta_{\max}) = 0\,.
\qquad (3.69)
$$

---

[9]Note: These assumptions are valid as long as $f_n(\eta)$ is bounded and is symmetric about its mean since a simple linear transformation may be used to shift the pdf to the origin.

Next, the expression $\partial J/\partial a_m$ is computed for $m \neq 0$ to find the coefficients $\{a_k\}$ which minimize J. Noting that $\int_{\eta\,\min}^{\eta\,\max} f_n{}'(\rho)\cos(m\omega_0\rho)d\rho = 0$ and $\int_{\eta\,\min}^{\eta\,\max} \sin(k\omega_0\rho)\cos(m\omega_0\rho)f_n(\rho)d\rho = 0$, the resulting system of equations is:

$$a_0\,E[\cos(m\omega_o n)] + \sum_{k=1}^{p} a_k\,\{E[\cos((k-m)\omega_o n)]$$
$$+ E[\cos((k+m)\omega_0 n)]\} = 0\,,\,m = 1,\ldots,p\,.$$

$$(3.70)$$

Finally, J is minimized with respect to $\{b_k\}$ by computing $\partial J/\partial b_k$ and equating it to zero. Using the facts that $f_n(\eta\,\min) = f_n(\eta\,\max)$ and $\sin(m\omega_0\eta\,\min) = \sin(m\omega_0\eta\,\max) = 0$,[10] the result is the following system of equations:

$$\tfrac{1}{2}\sum_{k=1}^{p} b_k\,\{E[\cos((k-m)\omega_0 n)] - E[\cos((k+m)\omega_0 n)]\}$$

$$= f_n(\eta\,\min)\sin(m\omega_0\eta\,\min) - f_n(\eta\,\max)\sin(m\omega_0\eta\,\max) \qquad (3.71)$$
$$+ m\omega_0 E[\cos(m\omega_0 n)]$$

$$= m\omega_0 E[\cos(m\omega_0 n)]$$

for $m = 1,\ldots,p$. To simplify notation, define the vectors

$$\mathbf{a} \doteq \begin{bmatrix} a_0 & a_1 & \ldots & a_p \end{bmatrix}^T$$

$$\mathbf{b} \doteq \begin{bmatrix} b_1 & b_2 & \ldots & b_p \end{bmatrix}^T$$

$$(3.72)$$

$$\mathbf{c} \doteq \begin{bmatrix} E\{\cos(\omega_0 n)\} \\ 2\,E\{\cos(2\omega_0 n)\} \\ \vdots \\ p\,E\{\cos(p\omega_0 n)\} \end{bmatrix},$$

<hr/>

[10]To see this, recall that $\omega_0 = 2\pi/(\eta_{max} - \eta_{min}) = \pi/\eta_{max} = -\pi/\eta_{min}$.

and the matrix

$$
\mathbf{T} \doteq \begin{bmatrix}
1 - E\{\cos(2\omega_0 n)\} & E\{\cos(\omega_0 n)\} \\ & -E\{\cos(3\omega_0 n)\} & \cdots & E\{\cos[(P-1)\omega_0 n]\} \\ & & & -E\{\cos[(P+1)\omega_0 n]\} \\[2mm]
E\{\cos(\omega_0 n)\} \\ -E\{\cos(3\omega_0 n)\} & 1 - E\{\cos(4\omega_0 n)\} & \cdots & E\{\cos[(P-2)\omega_0 n]\} \\ & & & -E\{\cos[(P+2)\omega_0 n]\} \\[2mm]
\vdots & & \ddots \\[2mm]
E\{\cos[(P-1)\omega_0 n]\} \\ -E\{\cos[(P+1)\omega_0 n]\} & \cdots & \cdots & 1 - E\{\cos(2P\omega_0 n)\}
\end{bmatrix} . \quad (3.73)
$$

Then, assuming T is invertible and that the set of equations described by Eq. (3.69) and Eq. (3.70) are linearly independent, the coefficients $\{a_k\}$ and $\{b_k\}$ which minimize J are found via the matrix equations

$$
\mathbf{a} = \mathbf{0}
$$

$$
\mathbf{b} = 2\omega_0 \, \mathbf{T}^{-1} \mathbf{c} . \qquad (3.74)
$$

Thus the resulting FSA estimate of $g(\rho)$ is given by (ignoring the $1/\rho$ term)

$$
\hat{g}(\rho) = \sum_{k=1}^{P} b_k \, \sin(k\omega_0 \rho) \qquad (3.75)
$$

for $\eta_{\min} \leq \rho \leq \eta_{\max}$ and 0 otherwise, where the set of coefficients $\{b_k\}$ is given by Eq. (3.74).

The previous derivations for the FSA estimate of a pdf (Section 3.4) and of the memoryless LO nonlinearity used the assumption that the noise pdf, $f_n(\eta)$, was bounded. However, there are many cases of interest in which the support of $f_n(\eta)$ is unbounded, e.g., the Gaussian pdf [12], Ch. 2). In these instances the FSA algorithm may still be used with the following modifications. The observed received signal in most applications will have a maximum and minimum value. If η_{max} is chosen as $\max(\mid \rho_{\max} \mid, \mid \rho_{\min} \mid)$, then the FSA estimate with $\omega_0 = \pi/\eta_{\max}$ will encompass all values of the received signal. However, the actual range of the pdf, $(-\infty, \infty)$, can be used to compute the coefficients via Eq. (3.55) or Eq. (3.74). While the result will not be a true estimate of the actual unbounded noise pdf, in most cases it will provide a suitable approximation given the fact that the range of observed received signal values is bounded.

The FSA algorithm can also be used for the case when the underlying pdf is unknown and knowledge of its domain (bounded or unbounded) is

unavailable. Provided that it is valid to assume that $f_n(\eta)$ is even-symmetric one can choose η_{max} as $\max(\mid \rho_{max} \mid, \mid \rho_{min} \mid)$. The required coefficients can then be computed using Eq. (3.56) for the pdf estimate, or Eq. (3.74) (substituting a sample average for the expectation operation) for a direct estimate of the LO nonlinearity.

Chapter 4

LO Detector with Memory Implementation Techniques

The implementation of a robust memoryless LO detector was the subject of Chapter 3. In this chapter two of these techniques, the histogram and kernel algorithms, are extended to the multidimensional problem of implementing a robust LO detector with memory. As before, pdf estimation algorithms are utilized to provide the framework by which the required LO nonlinearities of Eq. (2.8) and Eq. (2.9) can be estimated. The result is a detector that can be used in an unknown, and possible changing, interference environment.

As will be seen, the algorithms for implementing the LO nonlinearities with memory are more complicated than their memoryless counterparts. However, the algorithms with memory are potentially more powerful in that they utilize the interrelationship between data samples, whereas the memoryless algorithms process each sample independently. As a result, the LO detector with memory can be a prudent choice in environments characterized by highly correlated interference samples, such as channels containing narrowband jammers or noise sources modeled as *auto regressive* (AR) processes.

4.1 The Histogram Algorithm

While a histogram can be used to estimate a multivariate pdf, it is not particularly suited to the task of implementing the LO nonlinearities with

memory. This section presents the multivariate histogram algorithm and the reasons why it is not suited to the task of implementing the LO detector with memory.

Recall that the I and Q nonlinearities with memory of Eq. (2.8) and Eq. (2.9) are a function of $f_{\mathbf{n}_I \mathbf{n}_Q}(\boldsymbol{\eta}_I, \boldsymbol{\eta}_Q)$, the multivariate noise pdf. The histogram estimate of a multivariate pdf is a straightforward (but arduous) extension of the histogram algorithm for estimating univariate pdfs, discussed in Section 3.1. Let $\{\boldsymbol{\eta}_{I_i}\} = \{[\eta_{I_i}(1) \ldots \eta_{I_i}(N)]^T\}$ and $\{\boldsymbol{\eta}_{Q_i}\} = \{[\eta_{Q_i}(1) \ldots \eta_{Q_i}(N)]^T\}$ each be a set of L samples of the I and Q random noise vectors, $\mathbf{n}_I$ and $\mathbf{n}_Q$, each having length N. Define $\mathbf{n}^T = \begin{bmatrix} \mathbf{n}_I^T & \mathbf{n}_Q^T \end{bmatrix}$ as the concatenated random noise vector, and $\{\boldsymbol{\eta}_i^T\} = \left\{ \begin{bmatrix} \boldsymbol{\eta}_{I_i}^T & \boldsymbol{\eta}_{Q_i}^T \end{bmatrix} \right\}$ $= \{[\eta_{I_i}(1) \ldots \eta_{I_i}(N) \ \eta_{Q_i}(1) \ldots \eta_{Q_i}(N)]\} = \{[\eta_i(1) \ldots \eta_i(2N)]\}$ as the set of L samples of $\mathbf{n}$. Thus, $f_{\mathbf{n}_I \mathbf{n}_Q}(\boldsymbol{\eta}_I, \boldsymbol{\eta}_Q) = f_{\mathbf{n}}(\boldsymbol{\eta})$ is a $2N$-dimensional pdf.

Next, divide the domain of the jth dimension of $f_{\mathbf{n}}(\boldsymbol{\eta})$ into K regions using the breakpoints b_{jk}, where $j = 1, \ldots, 2N$ and $k = 0, \ldots, K$. Thus, the entire $2N$-dimensional support of $f_{\mathbf{n}}(\boldsymbol{\eta})$ is divided into K^{2N} "hyper-bins," $B_{k_1, \ldots, k_{2N}}$, defined as

$$B_{k_1, \ldots, k_{2N}} = \{\boldsymbol{\eta}_i : b_{jk_j} \leq \eta_i(j) < b_{j(k_j+1)} \text{ for } j = 1, \ldots, 2N$$

$$\text{(4.1)}$$

$$\text{and } k_j = 0, \ldots, K-1\}.$$

Note that the breakpoints $\{b_{jk}\}$ are chosen heuristically, e.g., such that each hyper-bin has the same width in each dimension, or each bin contains the same number of sample points.

The probability of a sample of the concatenated noise vector lying in a given bin, $P\{B_{k_1, \ldots, k_{2N}}\}$, is approximated by its relative frequency,

$$P\{B_{k_1, \ldots, k_{2N}}\} \approx \hat{P}\{B_{k_1, \ldots, k_{2N}}\} = \frac{1}{L} \sum_{i=1}^{L} I_{B_{k_1, \ldots, k_{2N}}}(\boldsymbol{\eta}_i) \qquad \text{(4.2)}$$

where $I_A(y)$ is the set indicator function. Finally, the multivariate histogram estimate of $f_{\mathbf{n}}(\boldsymbol{\eta})$, denoted as $\hat{f}_{\mathbf{n}}(\boldsymbol{\eta})$, is given by

$$\hat{f}_{\mathbf{n}}(\boldsymbol{\eta}) = \sum_{k_1=0}^{K-1} \cdots \sum_{k_{2N}=0}^{K-1} \frac{1}{C_{k_1, \ldots, k_{2N}}} \hat{P}\{B_{k_1, \ldots, k_{2N}}\} I_{B_{k_1, \ldots, k_{2N}}}(\boldsymbol{\eta}) \qquad \text{(4.3)}$$

where the normalizing scale factor, $C_{k_1,...,k_{2N}}$, is

$$C_{k_1,...,k_{2N}} = \prod_{j=1}^{2N} [b_{j(k_j+1)} - b_{jk_j}] . \tag{4.4}$$

At this point, the practicality of the multivariate histogram estimator of Eq. (4.3) should be discussed. Suppose that, on average, it is desired to have P samples in each hyper-bin. Then, roughly $P \cdot K^{2N}$ concatenated sample vectors, η_i, are required. The result is a required total number of individual noise samples, $\eta_i(j)$, approximately equal to $2NPK^{2N}$ to yield approximately P sample points in each hyper-bin. For example, if $K = 10$ bins per dimension, $P = 10$ samples per hyper-bin, and $N = 2$, i.e., $f_{\mathbf{n}_I \mathbf{n}_Q}(\boldsymbol{\eta}_i, \boldsymbol{\eta}_Q) = f_{n_I(1)n_I(2)n_Q(1)n_Q(2)}(\eta_I(1), \eta_I(2), \eta_Q(1), \eta_Q(2))$, then a total of approximately $400,000$ individual noise samples are required. If $N = 10$, however, approximately 2×10^{22} individual noise samples are required. As can be seen, a linear increase in the length of the I and Q noise vectors results in an exponential increase in the number of individual noise data samples. Since in most situations it is not possible to obtain the required large number of data samples, the resulting multivariate histogram estimate will be poor. An example of a 2-dimensional histogram estimate corresponding to iid Gaussian I and Q noise data, for $K = 6$ and $L = 10,000$, is shown in Fig. 4.1.

From the preceding discussion, it is evident that the multivariate histogram estimate will provide an extremely crude noise pdf estimate at best. Even for the example pdf in Fig. 4.1, with $P \approx 280$ samples per hyper-bin, the resulting estimate is poor. In addition, the numerical differentiation techniques required to produce the approximate gradient of the histogram estimate will introduce further error. Thus, a multivariate pdf estimation technique more suited to the implementation of the LO nonlinearities with memory is presented in the next section.

4.2 The Kernel Algorithm

The multivariate kernel estimator of the noise pdf is developed as follows. Define the concatenated noise vector $\mathbf{n}^T = \begin{bmatrix} \mathbf{n}_I^T \mathbf{n}_Q^T \end{bmatrix}$ and let $\{\boldsymbol{\eta}_i\} = \{[\eta_i(1)\eta_i(2)\ldots\eta_i(2N)]^T\}$, $i = 1,\ldots,L$, be a set of L samples of the random noise vector, $\mathbf{n}$. Since $\mathbf{n}$ has length $2N$, the total number of
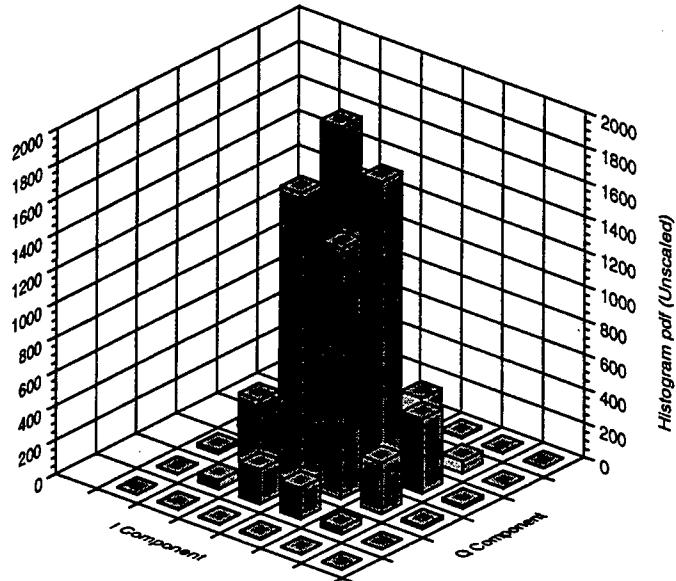
Figure 4.1: Example of a multivariate histogram estimate of a pdf - iid Gaussian I and Q data with $K = 6$ and $L = 10,000$.

available samples is $Q = 2LN$. The general multivariate kernel estimator is then defined as ([14], Ch. 6):

$$\hat{f}_{\mathbf{n}}(\boldsymbol{\eta}) = \frac{1}{L \mid \mathbf{H} \mid} \sum_{i=1}^{L} K(\mathbf{H}^{-1}(\boldsymbol{\eta} - \boldsymbol{\eta}_i)). \tag{4.5}$$

The window $K(\mathbf{t})$ is now a multivariate kernel and $\mathbf{H}$ is a linear transform matrix.

At this point a special form of the general multivariate kernel estimator will be presented: the product kernel estimator. The product kernel estimate of $f_{\mathbf{n}}(\boldsymbol{\eta})$ is ([14], Ch. 6):

$$\hat{f}_{\mathbf{n}}(\boldsymbol{\eta}) = \hat{f}_{\mathbf{n}}(\eta(1), .., \eta(j), .., \eta(2N)) = \frac{1}{L\, h_1 \cdots h_{2N}} \sum_{i=1}^{L} \left[\prod_{j=1}^{2N} K\left(\frac{\eta(j) - \eta_i(j)}{h_j} \right) \right] \tag{4.6}$$

where $\eta(j)$ is the jth argument of $f_{\mathbf{n}}(\boldsymbol{\eta})$ and $\eta_i(j)$ is the jth sample of the ith observed concatenated noise vector. The parameters $\{h_j\}$ are the smoothing parameters corresponding to each dimension of the kernel estimate. The kernel function $K(t)$ is the same univariate kernel discussed in Section 3.5.

57

Recall that the LO detector with memory requires the partial derivatives of the multivariate noise pdf. The product kernel estimate of $\frac{\partial}{\partial \eta(q)} f_{\mathbf{n}}(\boldsymbol{\eta})$ is found by differentiating $\hat{f}_{\mathbf{n}}(\boldsymbol{\eta})$ in Eq. (4.6). The result is

$$
\frac{\partial}{\partial \eta(q)} \hat{f}_{\mathbf{n}}(\boldsymbol{\eta}) \;=\; \frac{\partial}{\partial \eta_q} \frac{1}{L\, h_1 \cdots h_{2N}} \sum_{i=1}^{L} \left[\prod_{j=1}^{2N} K\left(\frac{\eta(j) - \eta_i(j)}{h_j} \right) \right] \tag{4.7}
$$

$$
\;=\; \frac{1}{L\, h_q\, h_1 \cdots h_{2N}} \sum_{i=1}^{L} \left[K'\left(\frac{\eta(q) - \eta_i(q)}{h_q} \right) \prod_{\substack{j=1 \\ j \neq q}}^{2N} K\left(\frac{\eta(j) - \eta_i(j)}{h_j} \right) \right].
$$

Note that the expression in Eq. (4.7) can be extended to partial derivatives of arbitrary order.

As in the case of the univariate kernel estimator, the product kernel estimator has a useful expression yielding the set $\{h_j\}$ which minimizes the AMISE. If a Gaussian kernel is used and $\mathbf{n}$ is a multivariate Gaussian vector with independent components, then the value of h_j which minimizes the AMISE of $\hat{f}_{\mathbf{n}}(\boldsymbol{\eta})$ is ([14], Ch. 6)

$$
h_j \;=\; \left(\frac{4}{2N + 2} \right)^{1/(2N+4)} \sigma_j\, L^{-1/(2N+4)} \tag{4.8}
$$

where σ_j^2 is the variance of the jth component of $\mathbf{n}$. Equation (4.8) provides a starting point for determining $\{h_j\}$ that is most suitable for the given application.

The product kernel estimate can be used to approximate the LO nonlinearity with memory by substituting the kernel estimates of $f_{\mathbf{n}}(\boldsymbol{\eta})$ and $\frac{\partial}{\partial \eta(q)} f_{\mathbf{n}}(\boldsymbol{\eta})$ ($q = 1, \ldots, 2N$) into Eq. (2.8) and Eq. (2.9), noting that $f_{\mathbf{n}}(\boldsymbol{\eta}) = f_{\mathbf{n}_I \mathbf{n}_Q}(\eta_I(1), \ldots, \eta_I(N), \eta_Q(1), \ldots, \eta_Q(N))$. The resulting product kernel estimate of $g_q(\boldsymbol{\rho}) = -\frac{\partial}{\partial \rho(q)} f_{\mathbf{n}}(\boldsymbol{\rho}) / f_{\mathbf{n}}(\boldsymbol{\rho})$ is:

$$
\hat{g}_q(\boldsymbol{\rho}) \;=\; -\frac{1}{h_q} \frac{\displaystyle\sum_{i=1}^{L} \left[K'\left(\frac{\rho(q) - \eta_i(q)}{h_q} \right) \prod_{\substack{j=1 \\ j \neq q}}^{2N} K\left(\frac{\rho(j) - \eta_i(j)}{h_j} \right) \right]}{\displaystyle\sum_{i=1}^{L} \left[\prod_{j=1}^{2N} K\left(\frac{\rho(j) - \eta_i(j)}{h_j} \right) \right]}. \tag{4.9}
$$

The techniques employed in arriving at Eq. (4.9) can be used to develop more sophisticated forms of the LO detector with memory.

4.3 Simulation Results

This section presents the simulation results for the product kernel implementation of the robust LO detector with memory. Results are presented for LO detection, with and without memory, in a standard QPSK system. In this case, the LO detector *without* memory refers to the detector of Eq. (2.13), in which successive noise samples are independent, but simultaneous I and Q samples are correlated. In implementing the LO nonlinearities, the following *critical* assumption is made: since the environments of interest exhibit high *jammer-to-signal* (J/S) *ratios, the received signal vector, $\mathbf{r}_I + j\mathbf{r}_Q$, is approximately equal to the noise vector, $\mathbf{n}_I + j\mathbf{n}_Q$, and thus $f_{\mathbf{r}_I \mathbf{r}_Q}(\cdot) \approx f_{\mathbf{n}_I \mathbf{n}_Q}(\cdot)$.* In other words, the received signal pdf was used in place of the noise pdf in the implementation of the LO nonlinearities.

The first scenario examined was the LO detector without memory in a QPSK system subjected to a single CW jammer. The P_b performance of the product kernel algorithm was determined relative to various values of J/S, f_j/R_s, and B, the *kernel resolution*. The parameter B is related to the smoothing parameters, $\{h_j\}$, by the following expression:

$$B = \frac{\rho_{jmax} - \rho_{jmin}}{h_j} \qquad (4.10)$$

where ρ_{jmax} and ρ_{jmin} are the maximum and minimum observed values of the received signal in the jth dimension, respectively. The resulting P_b plots are shown in Fig. 4.2 to Fig. 4.5, with the system parameters provided in Table 4.1.[1] As can be seen, the results for the LO detector without memory (but with correlated I and Q samples) exhibits a similar P_b characteristic as does the memoryless LO detector algorithms, whose results are provided in Section 3.6: P_b decreases as f_j/R_s increases. In addition, the kernel algorithm is also influenced by the value of B. For good performance in moderate J/S regions $(10dB < J/S < 20dB)$, B should be relatively small $(10 < B < 20)$. However, for good performance in large J/S regions $(20dB < J/S < 40dB)$,

---

[1] The results shown in the these figures were compiled from an average of five simulation runs.

B should be large ($20 < B < 40$). This corresponds to the discussion in Section 3.6, namely that h_j should be decreased as the noise environment becomes "less Gaussian." Thus, as J/S increases, the interference becomes "less Gaussian," and $B \propto 1/h_j$ must be increased.

System Parameters for the QPSK System		
	Parameter Name	Parameter Value
Transmitter and Receiver Parameters	Symbol rate (R_s) in Hz	0.05
	Samples per symbol (N)	20
	Memory length	1
	Kernel resolution (B)	10 to 40 by 10
	No. of samples per kernel approx. (Q)	1,000
Channel Parameters	J/S (in dB)	0 to 50 by 10
	f_j/R_s	0.00496 to 0.496 by 0.098208
	E_b/N_0 (in dB)	10
	Symbols used for P_b calculation	1,000

Table 4.1: System parameters for the product kernel algorithm (without memory) in a QPSK system: examination of P_b relative to J/S, f_j/R_s, and B.

The next scenario examined was the LO detector with memory in a QPSK system subjected to a single CW jammer. Specifically, the value of N chosen for the kernel algorithm was $N = 10$ (see Eq. (4.9)). The plots of P_b relative to J/S, f_j/R_s, and B are shown in Fig. 4.6 and Fig. 4.7, with the system parameters provided in Table 4.2.[2] As before, P_b was observed to decrease as f_j/R_s increased. Also, as J/S increased, an increase in B was also required to maintain a good value of P_b. However, the observed values of P_b for the LO detector with memory were typically larger than those for the LO detector without memory. The most probable reason for this phenomenon is the increase in error associated with approximating a pdf with a large dimensionality. The trade-off between memory length vs. approximation complexity will need to be addressed in future research.

From the analyses made in this section, as well as those in Section 3.6, it

---

[2]The results shown in the these figures were compiled from an average of five simulation runs.
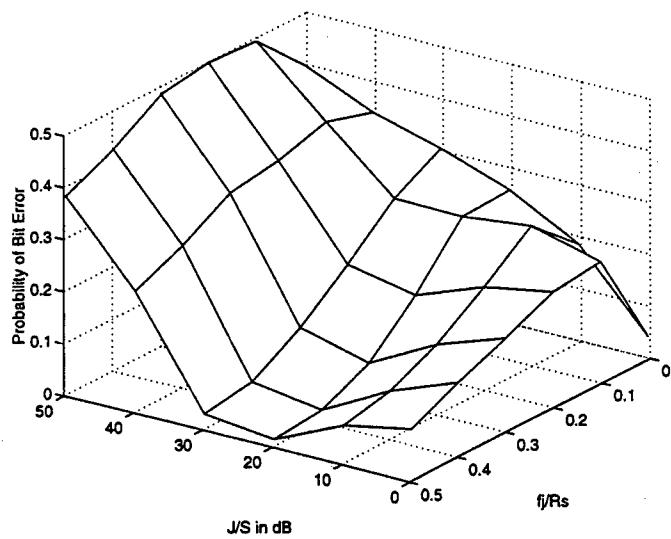
Figure 4.2: Probability of bit error (1 CW jammer) for the LO QPSK detector without memory simulation - $B = 10$
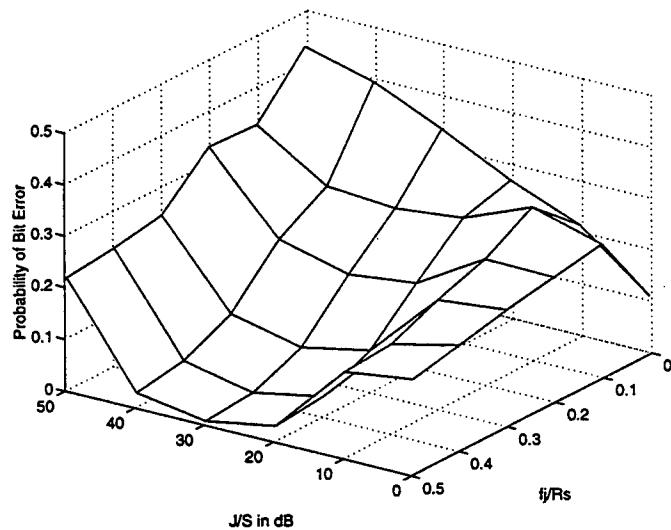
Figure 4.3: Probability of bit error (1 CW jammer) for the LO QPSK detector without memory simulation - $B = 20$
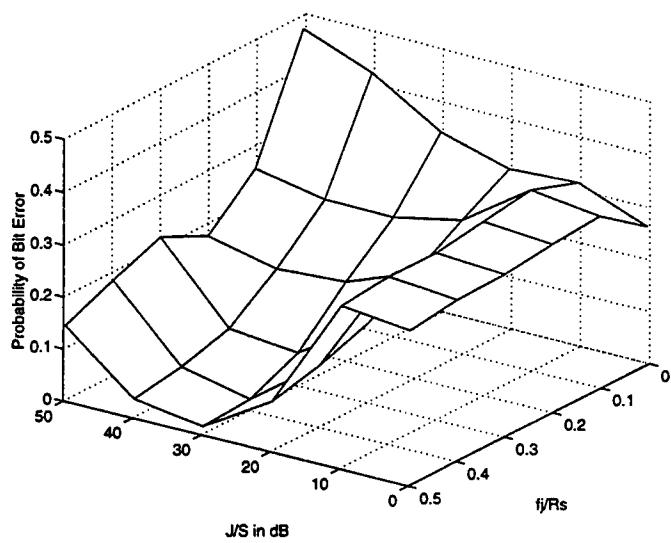
Figure 4.4: Probability of bit error (1 CW jammer) for the LO QPSK detector without memory simulation - $B = 30$
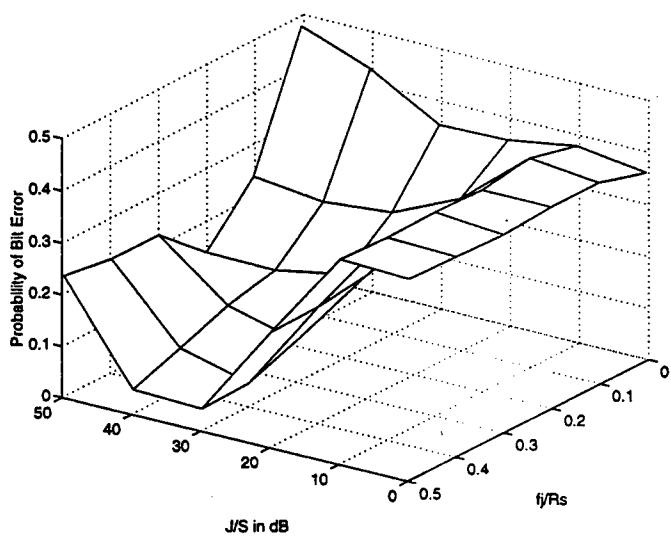
Figure 4.5: Probability of bit error (1 CW jammer) for the LO QPSK detector without memory simulation - $B = 40$

System Parameters for the QPSK System		
	Parameter Name	Parameter Value
Transmitter and Receiver Parameters	Symbol rate (R_s) in Hz	0.05
	Samples per symbol (N)	10
	Memory length	10
	Kernel resolution (B)	20 and 30
	No. of samples per kernel approx. (Q)	10,000
Channel Parameters	J/S (in dB)	0 to 50 by 10
	f_j/R_s	0.00496 to 0.496 by 0.098208
	E_b/N_0 (in dB)	10
	Symbols used for P_b calculation	1,000

Table 4.2: System parameters for the product kernel algorithm (with memory) in a QPSK system: examination of P_b relative to J/S, f_j/R_s, and B.
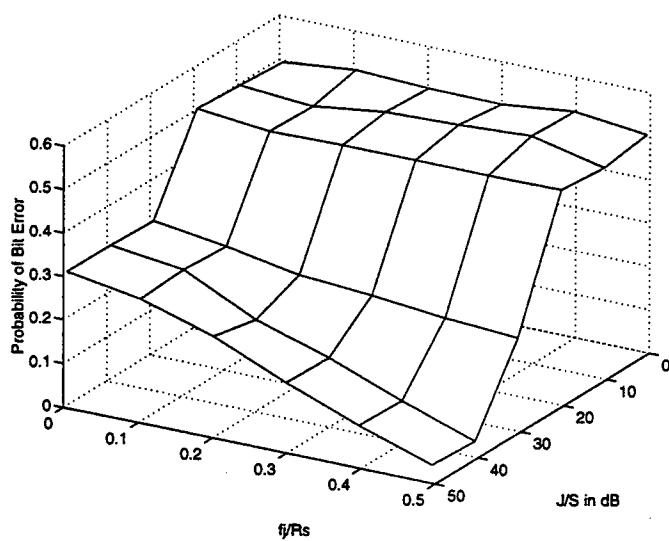

Figure 4.6: Probability of bit error (1 CW jammer) for the LO QPSK detector with memory simulation - $B = 20$
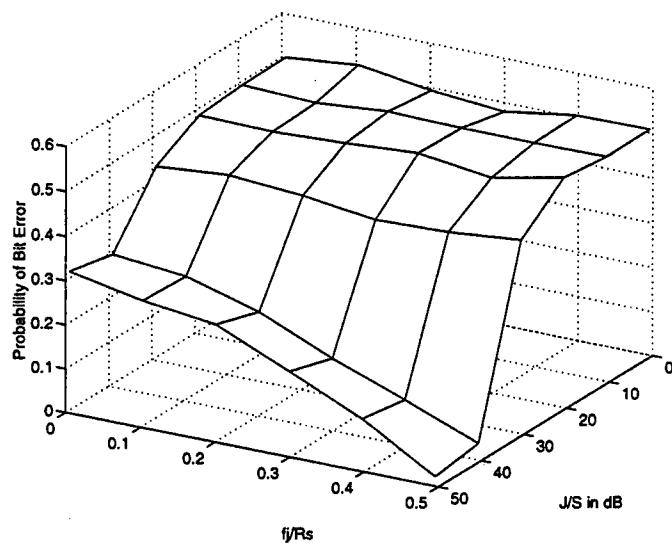
Figure 4.7: Probability of bit error (1 CW jammer) for the LO QPSK detector with memory simulation - $B = 30$

can be concluded that the LO detectors derived using the large J/S assumption that the *received signal pdf is approximately equal to the noise pdf* are not as robust as would be desired. The effect(s) of this assumption, as well as possible methods for improving performance, are discussed in the next chapter.

Chapter 5

"Ideal" Detection Techniques

The simulation analyses of the LO detector techniques discussed in Chapters 3 and 4 indicate that performance varies greatly depending on the jammer characteristics. In particular, for the case of a single CW jammer, all of the LO detector implementations exhibited the same trend in P_b: P_b increased when f_j/R_s decreased, i.e., a degradation in P_b was observed when the CW jammer occurred near the center of the main lobe of the information signal's frequency spectrum.

However, the goal of the robust LO detector is to provide reliable detection in a wide range of possible interference scenarios. In an effort to determine the cause(s) behind the observed decrease in performance, two *ideal* detector algorithms were examined: the *globally optimum* (GO) and the *ideal LO* (ILO) detectors. These two detector schemes are ideal in the sense that uncorrupted noise samples are assumed to be available at the receiver. Thus, by examining these two detector algorithms, the effects of the large J/S assumption that $f_{n_I n_Q}(\cdot) \approx f_{r_I r_Q}(\cdot)$ can be further investigated.

5.1 The Globally Optimum Detector

The GO detector for a standard QPSK system is a direct implementation of the ML detector for the signal and additive noise scenario, i.e.,

Choose the transmitted signal pair, (s_{I_m}, s_{Q_m}), which maximizes

$$f_{n_I n_Q}(\rho_I - s_{I_m}, \rho_Q - s_{Q_m}),$$

(5.1)

65

where $f_{\mathbf{n}_I \mathbf{n}_Q}(\boldsymbol{\eta}_I, \boldsymbol{\eta}_Q)$ is the joint pdf of the noise, $\mathbf{n}_I + j\mathbf{n}_Q$, and $\boldsymbol{\rho}_I + j\boldsymbol{\rho}_Q$ is the observed value of the received signal vector. The robust GO detector can be implemented using the multivariate kernel estimator discussed in Section 4.2. Define $\mathbf{n}$ as the concatenated random noise vector, $\mathbf{n}^T = \begin{bmatrix} \mathbf{n}_I^T \ \mathbf{n}_Q^T \end{bmatrix}$, and define $\{\boldsymbol{\eta}_i^T\} = \left\{ \begin{bmatrix} \boldsymbol{\eta}_{I_i}^T \ \boldsymbol{\eta}_{Q_i}^T \end{bmatrix} \right\}$ to be the set of L vectors formed by concatenating L observed samples of the I and Q channel noise vectors, each with length N. Then, $\boldsymbol{\eta}_i = [\eta_{I_i}(1) \dots \eta_{I_i}(N) \ \eta_{Q_i}(1) \dots \eta_{Q_i}(N)]^T$. The total number of available noise samples is thus $Q = 2LN$ Finally, defining the following vectors, $\boldsymbol{\rho}^T = \begin{bmatrix} \boldsymbol{\rho}_I^T \ \boldsymbol{\rho}_Q^T \end{bmatrix}$ and $\mathbf{s}_m^T = \begin{bmatrix} \mathbf{s}_{I_m}^T \ \mathbf{s}_{Q_m}^T \end{bmatrix}$, and using the result in Eq. (4.6), the product kernel implementation of the robust GO detector is

Choose $\mathbf{s}_m$ which maximizes

$$\hat{f}_{\mathbf{n}}(\boldsymbol{\rho} - \mathbf{s}_m) = \frac{1}{L h_1 \dots h_N} \sum_{i=1}^{L} \left[\prod_{j=1}^{2N} K \left(\frac{\rho(j) - s_m(j) - \eta_i(j)}{h_j} \right) \right]$$

(5.2)

or, more explicitly,

Choose the transmitted signal pair, $(\mathbf{s}_{I_m}, \mathbf{s}_{Q_m})$, which maximizes

$$\hat{f}_{\mathbf{n}_I \mathbf{n}_Q}(\boldsymbol{\rho}_I - \mathbf{s}_{I_m}, \boldsymbol{\rho}_Q - \mathbf{s}_{Q_m}) = \frac{1}{L h_{I_1} \dots h_{I_N} h_{Q_1} \dots h_{Q_N}}$$

$$\cdot \sum_{i=1}^{L} \left[\prod_{j=1}^{N} K \left(\frac{\rho_I(j) - s_{I_m}(j) - \eta_{I_i}(j)}{h_{I_j}} \right) \right.$$

$$\left. \cdot \prod_{j=1}^{N} K \left(\frac{\rho_Q(j) - s_{Q_m}(j) - \eta_{Q_i}(j)}{h_{Q_j}} \right) \right] .$$

(5.3)

In Eq. (5.2) and Eq. (5.3), h_j is the jth smoothing parameter in the sequence $\{h_{I_1}, \dots, h_{I_N}, h_{Q_1}, \dots, h_{Q_N}\}$ where h_{I_j} and h_{Q_j} are the smoothing parameters for the jth dimension of the I and Q noise vectors, respectively; $\eta_I(j)$ is the jth sample of the ith observed concatenated noise vector, $\boldsymbol{\eta}_i$, and correspondingly, $\eta_{I_i}(j)$ and $\eta_{Q_i}(j)$ are the jth samples of the ith observed I and Q noise vectors, respectively; and finally, $K(\cdot)$ is any one of a number of kernel windows discussed in Section 4.2 and [14], with the choice of kernel determined by the requirements specific to the given application.

It should be noted that, in general, the GO detector cannot be implemented in practice since it requires uncorrupted samples of the channel noise,

i.e., $\{\eta_{I_i}(j), \eta_{Q_i}(j)\}$, which are typically unavailable at the receiver in a communications system. However, the analysis of this detector will provide useful information concerning: (1) the attainable performance bounds of the robust detectors, (2) the effects of pdf estimation on detector implementation, and (3) the implications, and inaccuracies, associated with the assumption that $f_{\mathbf{n}_I\mathbf{n}_Q}(\cdot) \approx f_{\mathbf{r}_I\mathbf{r}_Q}(\cdot)$ in a high J/S environment.

5.2   The Ideal LO Detector

Recall from Eq. (2.7) that the general form of the LO detector with memory for quadrature signaling is given by:

Choose the possible signal pair, $(\mathbf{s}_{I_m}, \mathbf{s}_{Q_m})$, which maximizes:

$$l(\rho_I, \rho_Q) = \sum_{k=1}^{N} \left[s_{I_m}(k) g_{I_k}(\rho_I, \rho_Q) + s_{Q_m}(k) g_{Q_k}(\rho_I, \rho_Q) \right] \qquad (5.4)$$

where

$$g_{I_k}(\rho_I, \rho_Q) = \frac{\frac{\partial}{\partial \rho_I(k)} f_{\mathbf{n}_I\mathbf{n}_Q}(\rho_I, \rho_Q)}{f_{\mathbf{n}_I\mathbf{n}_Q}(\rho_I, \rho_Q)} \qquad (5.5)$$

and

$$g_{Q_k}(\rho_I, \rho_Q) = \frac{\frac{\partial}{\partial \rho_Q(k)} f_{\mathbf{n}_I\mathbf{n}_Q}(\rho_I, \rho_Q)}{f_{\mathbf{n}_I\mathbf{n}_Q}(\rho_I, \rho_Q)} \qquad (5.6)$$

are the ILO nonlinearities with memory. Using the result given in Eq. (4.9), and the definitions in the previous section, the product kernel implementations of $g_{I_k}(\rho_I, \rho_Q)$ and $g_{Q_k}(\rho_I, \rho_Q)$ are given by

$$\hat{g}_{I_k}(\rho_I, \rho_Q) = \frac{\sum_{i=1}^{L} \left\{ K' \left(\frac{\rho_I(k) - n_{I_i}(k)}{h_{I_k}} \right) \prod_{\substack{j=1 \\ j \neq k}}^{N} K \left(\frac{\rho_I(j) - n_{I_i}(j)}{h_{I_j}} \right) \prod_{j=1}^{N} K \left(\frac{\rho_Q(j) - n_{Q_i}(j)}{h_{Q_j}} \right) \right\}}{h_{I_k} \sum_{i=1}^{L} \left\{ \prod_{j=1}^{N} K \left(\frac{\rho_I(j) - n_{I_i}(j)}{h_{I_j}} \right) \prod_{j=1}^{N} K \left(\frac{\rho_Q(j) - n_{Q_i}(j)}{h_{Q_j}} \right) \right\}}$$

$$(5.7)$$

and

$$\hat{g}_{Q_k}(\rho_I, \rho_Q) = \frac{\sum_{i=1}^{L} \left\{ K' \left(\frac{\rho_Q(k) - n_{Q_i}(k)}{h_{Q_k}} \right) \prod_{j=1}^{N} K \left(\frac{\rho_I(j) - n_{I_i}(j)}{h_{I_j}} \right) \prod_{\substack{j=1 \\ j \neq k}}^{N} K \left(\frac{\rho_Q(j) - n_{Q_i}(j)}{h_{Q_j}} \right) \right\}}{h_{Q_k} \sum_{i=1}^{L} \left\{ \prod_{j=1}^{N} K \left(\frac{\rho_I(j) - n_{I_i}(j)}{h_{I_j}} \right) \prod_{j=1}^{N} K \left(\frac{\rho_Q(j) - n_{Q_i}(j)}{h_{Q_j}} \right) \right\}}$$

$$(5.8)$$

where ($'$) denotes differentiation.

As with the GO detector, the ILO detector is not usually implementable since it requires uncorrupted samples of the channel noise. However, the ILO detector can be utilized to determine performance bounds, as well as limitations associated with LO detector implementations that use the received signal samples as approximations of the noise.

5.3 Simulation Results

This section presents the simulation results for the GO and ILO detectors discussed in Sections 5.1 and 5.2. The main objective behind examining these two detector structures is twofold: (1) to determine the theoretical performance limits for the robust LO detector, and (2) to determine the effect on P_b of the large J/S assumption that *the noise pdf can be approximated by the received signal pdf.*

The P_b results for the robust GO detector in a standard QPSK system subjected to a single CW jammer are shown in Fig. 5.1 to Fig. 5.3, with the system parameters given in Table 5.1.[1] In these figures, P_b is shown relative to various values of J/S, f_j/R_s, and B. As can be seen, for a given value of J/S, and almost *any* f_j/R_s, P_b can be reduced to useful value through a judicious choice of B. In particular, for low J/S ($-20dB < J/S < 10dB$), a small value of B ($B \approx 10$) is required. For high J/S ($20dB < J/S < 40dB$) a larger value of B ($20 < B < 30$) is required. These results support the assertion that the value of B in the kernel method must be increased as the noise becomes "less Gaussian." While the plots for the GO detector show that f_j/R_s has little effect on P_b (for appropriate B and J/S regions), the same was not observed for the LO detector (see Section 3.6). Instead, P_b for the LO detector increased as f_j/R_s decreased. Thus, the observed performance of the two detectors indicates that the GO detector is more robust than the standard LO detector.

Next, the performance of the GO detector was examined for the case of a

---

[1]The results shown in the these figures were compiled from only a single simulation run. Thus, these graphs should be used for the purpose of determining performance trends, and not quantitative values of P_b. Also, in many cases the resulting calculated value of P_b was equal to zero. However, since P_b was computed using only 1,000 symbols, a value of zero actually corresponds to a P_b on the order of 10^{-3} or less.

System Parameters for the QPSK System		
	Parameter Name	Parameter Value
Transmitter and Receiver Parameters	Symbol rate (R_s) in Hz	0.05
	Samples per symbol (N)	10
	Memory length	10
	Kernel resolution (B)	10 to 30 by 10
	No. of samples per kernel approx. (Q)	10,000
Channel Parameters	J/S (in dB)	-20 to 50 by 10
	f_j/R_s	0.00496 to 0.496 by 0.098208
	E_b/N_0 (in dB)	10
	Symbols used for P_b calculation	1,000

Table 5.1: System parameters for the GO detector in a QPSK system subjected to a single CW jammer: examination of P_b relative to J/S, f_j/R_s, and B.
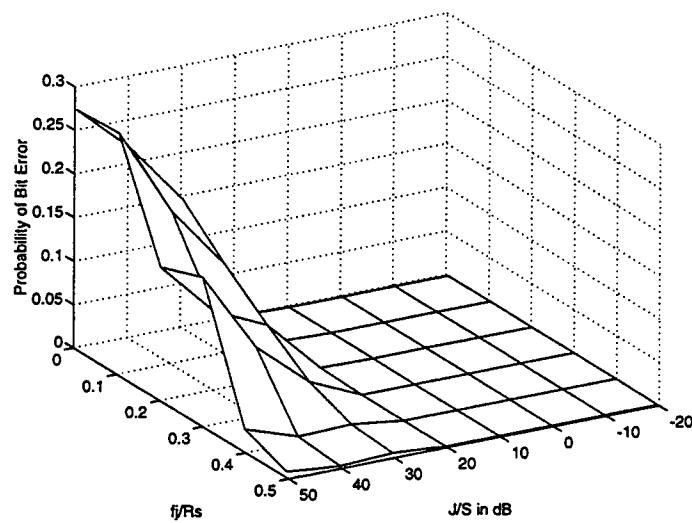

Figure 5.1: Probability of bit error (1 CW jammer) for the GO QPSK detector with memory simulation - $B = 10$
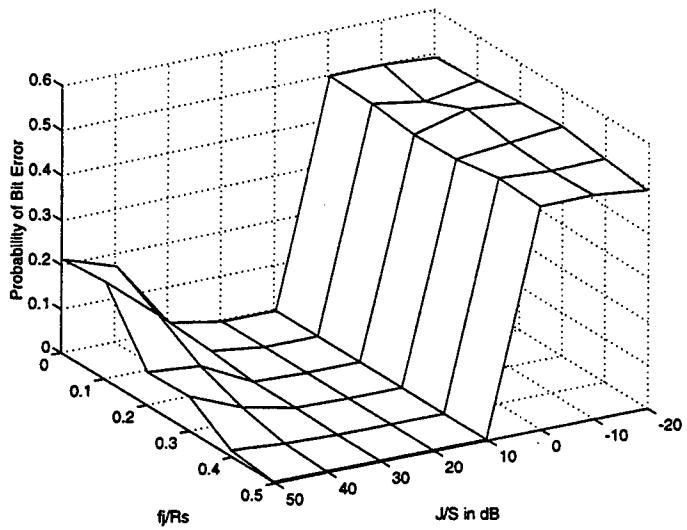
Figure 5.2: Probability of bit error (1 CW jammer) for the GO QPSK detector with memory simulation - $B = 20$
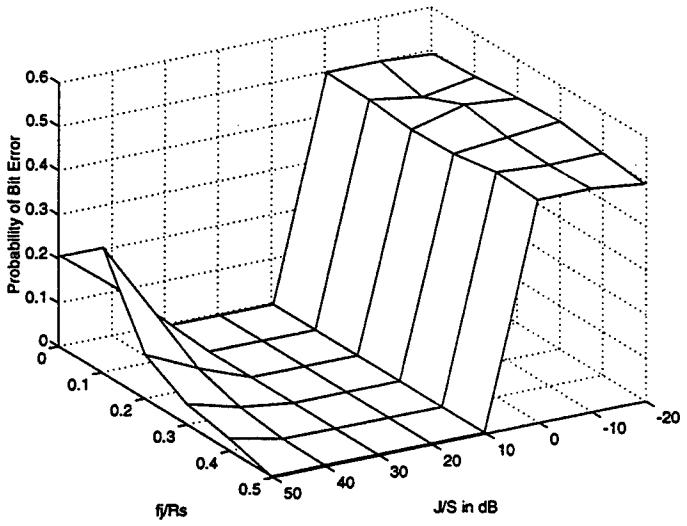

Figure 5.3: Probability of bit error (1 CW jammer) for the GO QPSK detector with memory simulation - $B = 30$

QPSK system subjected to two CW jammers. Specifically, the first jammer was fixed at $J/S = 30dB$ and $f_j/R_s = 0.496$, with the second jammer allowed to vary. The corresponding P_b plots, for the system parameters in Table 5.2, are provided in Fig. 5.4 to Fig. 5.6.[2] These figures show that good P_b performance can be attained for a wide variety of J/S and f_j/R_s second jammer configurations. Previous work [5], however, has shown that the standard robust LO detector does not perform well when subjected to two CW jammers, except when one has a low J/S, e.g., $J/S < 0dB$.

System Parameters for the QPSK System		
	Parameter Name	Parameter Value
Transmitter and Receiver Parameters	Symbol rate (R_s) in Hz	0.05
	Samples per symbol (N)	10
	Memory length	10
	Kernel resolution (B)	10 to 30 by 10
	No. of samples per kernel approx. (Q)	10,000
Channel Parameters	J/S (in dB) for 1st jammer	30
	f_j/R_s for 1st jammer	0.496
	J/S (in dB) for 2nd jammer	-20 to 50 by 10
	f_j/R_s for 2nd jammer	0.00406 to 0.406 by 0.080388
	E_b/N_0 (in dB)	10
	Symbols used for P_b calculation	1,000

Table 5.2: System parameters for the GO detector in a QPSK system subjected to two CW jammers: examination of P_b relative to J/S, f_j/R_s, and B.

---

[2]The results shown in the these figures were compiled from only a single simulation run. Thus, these graphs should be used for the purpose of determining performance trends, and not quantitative values of P_b. Also, in many cases the resulting calculated value of P_b was equal to zero. However, since P_b was computed using only 1,000 symbols, a value of zero actually corresponds to a P_b on the order of 10^{-3} or less.
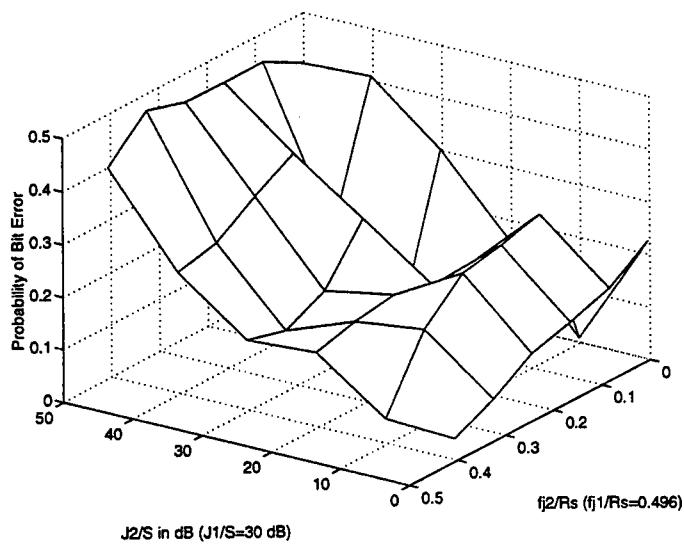
Figure 5.4: Probability of bit error (2 CW jammers) for the GO QPSK detector with memory simulation - $B = 10$
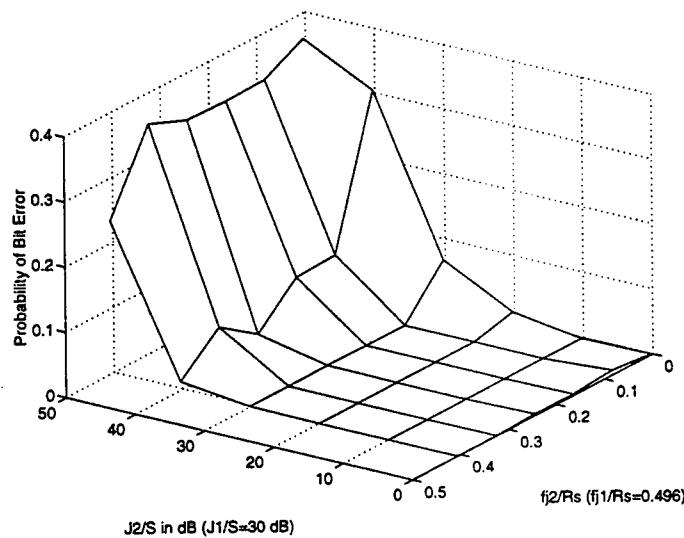

Figure 5.5: Probability of bit error (2 CW jammers) for the GO QPSK detector with memory simulation - $B = 20$
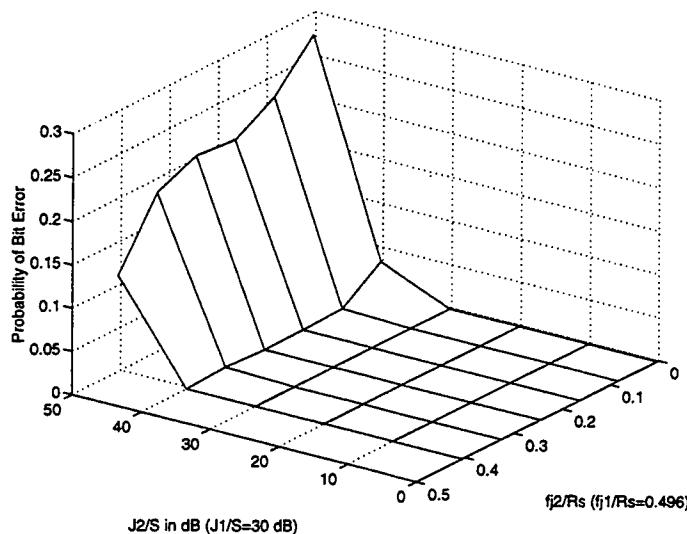
Figure 5.6: Probability of bit error (2 CW jammers) for the GO QPSK detector with memory simulation - $B = 30$

Finally, the performance of the GO detector in a QPSK system subjected to three CW jammers was examined. In this case, the first jammer was fixed at $J/S = 30dB$ and $f_j/R_s = 0.496$, the second at $J/S = 30dB$ and $f_j/R_s = 0.496$, and the third was varied. The plots of P_b relative to J/S and f_j/R_s for the third jammer, as well as various values of B, are provided in Fig. 5.7 to Fig. 5.9.[3] The corresponding system parameters are listed in Table 5.3. These results, as before, indicate that a low value of P_b can be attained for a wide range of J/S and f_j/R_s settings through judicious choice of B.

The P_b performance of the ideal robust LO detector was also examined. Specifically, P_b for the ILO detector in a QPSK system subjected to a single CW jammer is plotted in Fig. 5.10 through Fig. 5.12, with the system pa-

---

[3]The results shown in the these figures were compiled from only a single simulation run. Thus, these graphs should be used for the purpose of determining performance trends, and not quantitative values of P_b. Also, in many cases the resulting calculated value of P_b was equal to zero. However, since P_b was computed using only 1,000 symbols, a value of zero actually corresponds to a P_b on the order of 10^{-3} or less.

System Parameters for the QPSK System		
	Parameter Name	Parameter Value
Transmitter **and** **Receiver** **Parameters**	Symbol rate (R_s) in Hz	0.05
	Samples per symbol (N)	10
	Memory length	10
	Kernel resolution (B)	15 to 35 by 10
	No. of samples per kernel approx. (Q)	10,000
Channel **Parameters**	J/S (in dB) for 1st jammer	30
	f_j/R_s for 1st jammer	0.496
	J/S (in dB) for 2nd jammer	30
	f_j/R_s for 2nd jammer	0.406
	J/S (in dB) for 3rd jammer	-20 to 50 by 10
	f_j/R_s for 3rd jammer	0.00456 to 0.456 by 0.090288
	E_b/N_0 (in dB)	10
	Symbols used for P_b calculation	1,000

Table 5.3: System parameters for the GO detector in a QPSK system subjected to three CW jammers: examination of P_b relative to J/S, f_j/R_s, and B.
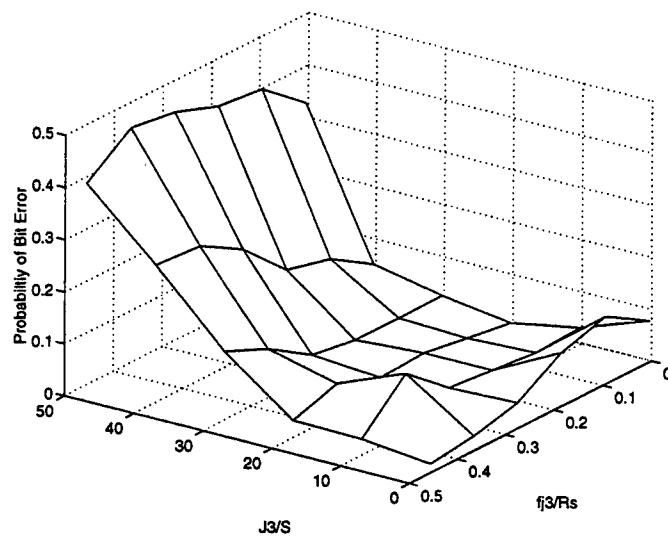
Figure 5.7: Probability of bit error (3 CW jammers) for the GO QPSK detector with memory simulation - $B = 15$
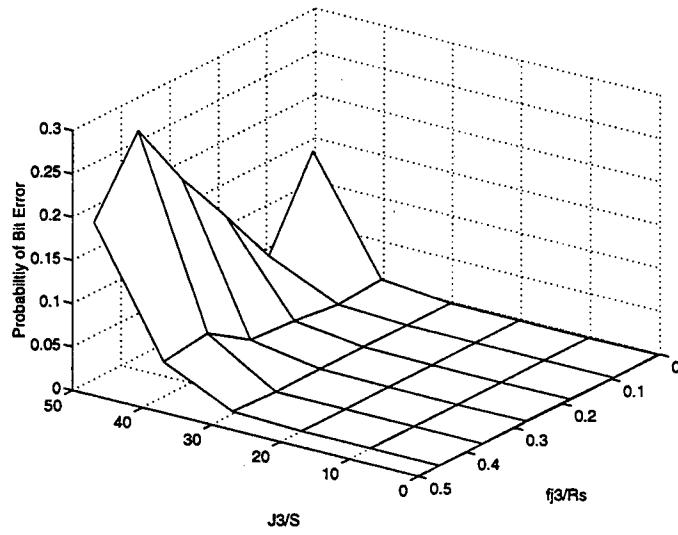
Figure 5.8: Probability of bit error (3 CW jammers) for the GO QPSK detector with memory simulation - $B = 25$

75
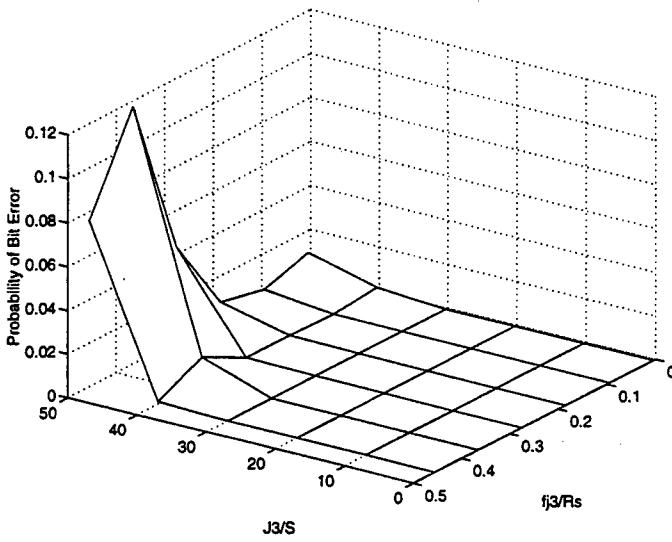
Figure 5.9: Probability of bit error (3 CW jammers) for the GO QPSK detector with memory simulation - $B = 35$

rameters given in Table 5.4.[4] As can be seen, P_b for the ideal LO detector is similar to that for the GO detector (see Fig. 5.1 to Fig. 5.3), and as before, an increase in J/S requires an increase in B in order to yield good performance. However, in some regions, particularly those characterized by low J/S, the performance of the ideal LO detector is poorer than that of the GO detector. This is most likely due to two reasons: (1) because of computational constraints, only 1,000 samples were used in each ideal LO nonlinearity estimate, whereas 10,000 samples were used in each GO detector approximation, and (2) the large interfence requirement used in the derivation of the LO detector is not met when J/S is small, resulting in a poor approximation to the optimum, or GO, detector in these regions.

The results in this section illustrate a number of important points. First, the instances of large P_b for the LO detector, observed in Sections 3.6 and

---

[4]The results shown in the these figures were compiled from only a single simulation run. Thus, these graphs should be used for the purpose of determining performance trends, and not quantitative values of P_b. Also, in many cases the resulting P_b was equal to zero. However, since P_b was computed using only 1,000 symbols, a value of zero actually corresponds to a P_b on the order of 10^{-3} or less.

System Parameters for the QPSK System		
	Parameter Name	Parameter Value
Transmitter **and** **Receiver** **Parameters**	Symbol rate (R_s) in Hz	0.05
	Samples per symbol (N)	10
	Memory length	10
	Kernel resolution (B)	10 to 30 by 10
	No. of samples per kernel approx. (Q)	1,000
Channel **Parameters**	J/S (in dB)	-20 to 50 by 10
	f_j/R_s	0.00496 to 0.496 by 0.098208
	E_b/N_0 (in dB)	10
	Symbols used for P_b calculation	1,000

Table 5.4: System parameters for the ILO detector in a QPSK system subjected to a single CW jammer: examination of P_b relative to J/S, f_j/R_s, and B.
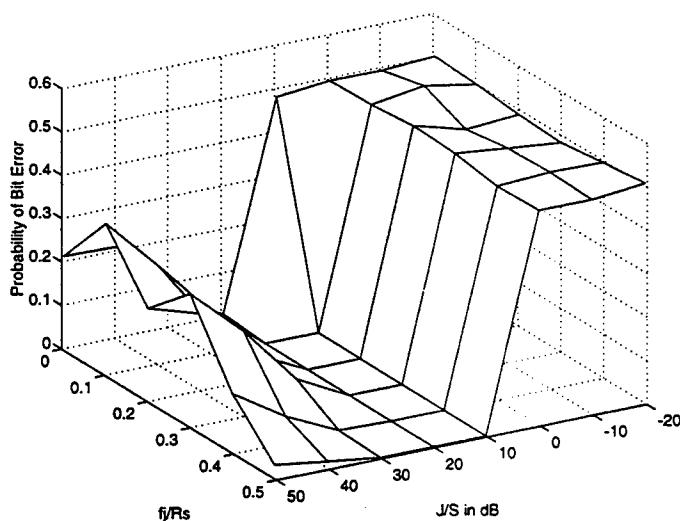

Figure 5.10: Probability of bit error (1 CW jammer) for the *ideal* LO QPSK detector with memory simulation - $B = 10$
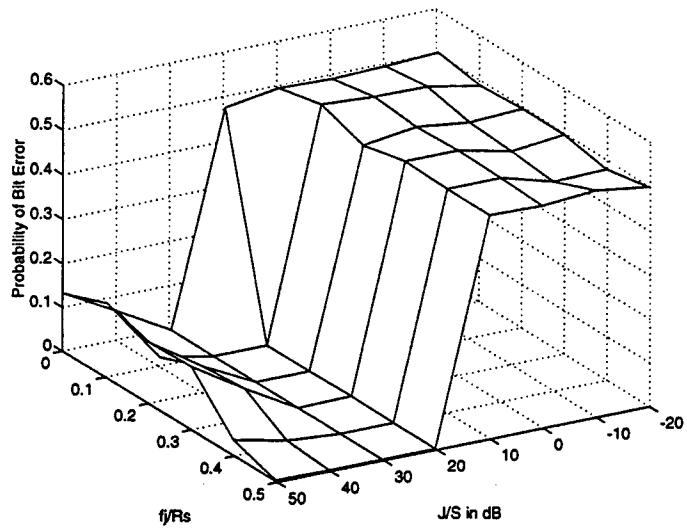
Figure 5.11: Probability of bit error (1 CW jammer) for the *ideal* LO QPSK detector with memory simulation - $B = 20$
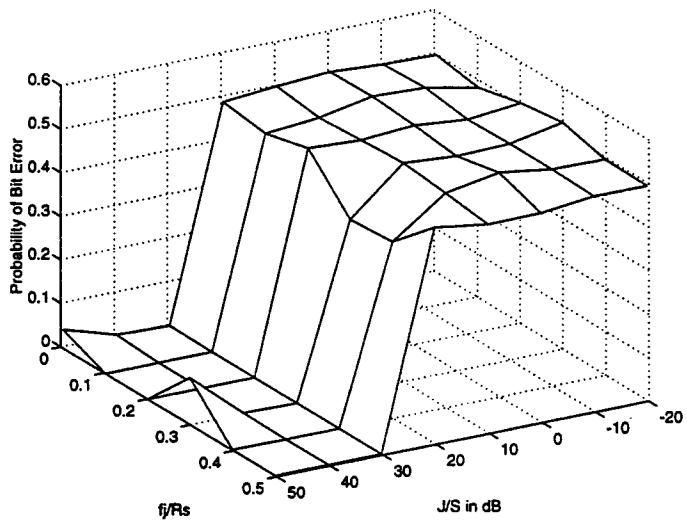

Figure 5.12: Probability of bit error (1 CW jammer) for the *ideal* LO QPSK detector with memory simulation - $B = 30$

78

4.3, most likely can *not* be attributed to error in the nonlinearity approximations since these same estimation techniques were used in the GO and ILO detectors. Second, for the robust LO detector in a system subjected to CW jammers, the increase in P_b corresponding to a decrease in f_j/R_s is *not* inherent in the defining expression, Eq. (2.7), for the LO detector, as this trend was not observed in the P_b results for the ILO detector. Finally, the large J/S assumption that the *noise pdf can be approximated by the received signal pdf* is the most likely cause of the LO detector's regions of poor performance, because this is the only significant difference between the LO detector and the GO/ILO detector algorithms. Thus, it can be hypothesized that improvements in the performance of the robust LO detector can be attained by constructing, at the receiver, good estimates of the noise samples, or an accurate estimate of the noise pdf.

Chapter 6

Summary

The focus of this report has been robust *locally optimum* (LO) detection in a communications system subjected to interference exhibiting a large *jammer-to-signal ratio* (J/S). The term *robust*, in this context, indicates that prior information regarding the channel statistics is not required. Instead, the LO nonlinearity is implemented using an estimate of the channel noise *probability density function* (pdf). Thus, the robust LO detector can be used in applications where the channel interference is unknown and possibly nonstationary.

A derivation of the various LO detector structures was provided in Chapter 2. In particular, LO detection in a quadrature signaling environment was examined, with emphasis on a *quadrature phase shift keyed* (QPSK) *direct sequence* (DS) *spread spectrum* (SS) system. There are three forms of LO detection: (1) detection with memory, (2) detection in *independent and identically distributed* (iid) noise, and (3) memoryless detection. In LO detection with memory, no assumptions concerning the noise pdf are made, and thus the entire multivariate pdf is used in constructing the LO nonlinearity. LO detection in iid noise utilizes the assumption that successive noise samples are iid, but with simultaneous *in-phase* (I) and *quadrature* (Q) samples remaining correlated. This detector structure, therefore, utilizes the two-dimensional joint pdf of the I and Q channel noise to construct the LO nonlinearity. Finally, in memoryless detection the noise is assumed to be iid, and the noise pdf is assumed to possess radial symmetry. In this case, only the univariate pdf of the noise magnitude is required to implement the LO nonlinearity.

With the derivations of the various LO detector structures completed,

Chapter 3 focused on the implementation of the memoryless LO detector. Five techniques, which utilize estimates of the noise pdf and its derivative, were presented. These methods are: (1) the histogram algorithm, (2) the *M-interval polynomial approximation* (MIPA), (3) the *continuous polynomial approximation* (CPA), (4) the *Fourier series approximation* (FSA), and (5) the kernel algorithm. In all of these methods, observed samples of the channel noise are used to estimate the noise pdf and its derivative, from which an estimate of the memoryless LO nonlinearity is constructed. However, in most applications uncorrupted noise samples are unavailable, e.g, *the noise is corrupted by the information signal*. A common solution is to employ the large J/S assumption that *the noise pdf is approximately equal to the received signal pdf*. The results in Section 3.6 illustrate that this assumption is not always valid, even in high J/S environments.

The robust LO detector with memory was the subject of Chapter 4. Two methods of implementing the detector were presented: (1) the histogram, and (2) the kernel algorithms. The histogram algorithm was shown to be unsuitable for the task of implementing the LO nonlinearity with memory since it requires an extremely large number of observations to construct a useful pdf estimate. The kernel algorithm, on the other hand, was shown to be well-suited to this task. As before, since uncorrupted noise samples are usually unavailable, the large J/S assumption that the noise pdf can be approximated by the received signal pdf was utilized. The simulation results in Section 4.3 indicated that, as for the memoryless case, this assumption is not always valid.

The simulation results for the robust LO detectors with and without memory implied that these detectors are not as robust as would be desired. To determine the cause of the observed regions of poor performance, two "ideal" detector structures were examined in Chapter 5: (1) the *globally optimum* (GO), and (2) the *ideal LO* (ILO) detectors. In both of these detector algorithms, uncorrupted noise samples, although unavailable in practice, were provided and used to estimate the required noise pdfs. The simulation results showed that both of these techniques provided "robust" performance over a wide range of jamming scenarios. Thus, it can be *inferred* that the poor performance regions of the various LO detector algorithms were caused by the use of the large J/S assumption that *the noise pdf is approximately equal to the received signal pdf*.

In conclusion, robust LO detection techniques can be extremely useful in

applications characterized by unknown, nonstationary interference, provided that an accurate estimate of the noise pdf can be made. Thus, techniques for either obtaining uncorrupted estimates of the noise samples, or for constructing an accurate estimate of the noise pdf from a preliminary estimate of the received signal pdf, will be required in order to take full advantage of the "robustness" available in the robust LO detector.

Bibliography

[1] J. Capon, "On the Asymptotic Efficiency of Locally Optimum Detectors," *IRE Transactions on Information Theory*, pp. 67-71, April 1961.

[2] D. Middleton, "Canonically Optimum Threshold Detection," *IEEE Transactions on Information Theory*, Vol. IT -12, No. 2, pp. 230-243, April 1966.

[3] W. Gardner, "Structural Characterization of Locally Optimum Detectors in Terms of Locally Optimum Estimators and Correlators," *IEEE Transactions on Information Theory*, Vol. IT-28, No. 6, pp. 924-932, November 1982.

[4] S. A. Kassam, *Signal Detection in Non-Gaussian Noise*, New York: Springer-Verlag, 1988.

[5] D. R. Ucci, W. E. Jacklin, and J. G. Grimm, *Investigation and Simulation of Nonlinear Processors for Spread Spectrum Receivers*, Final Technical Report for Rome Laboratory, USAF, Report No. RL-TR-93-258, 1993.

[6] W. E. Jacklin, J. H. Grimm, and D. R. Ucci, "The Simulation of a Two-Dimensional Spread Spectrum System with Locally Optimal Processing," *Proceedings of the 1993 IEEE MILCOM Conference*, pp. 288-292, 1993.

[7] J. H. Grimm, et. al., "Continuous Polynomial Approximation," *Proceedings of the 1993 IEEE MILCOM Conference*, pp. 283-287, October 1993.

[8] D. R. Ucci, W. E. Jacklin, and J. G. Grimm, *A Spread Spectrum Receiver with Nonlinear Processing*, Final Technical Report for Rome Laboratory, USAF, Report No. RL-TR-93-50, 1993.

* [9] Hazeltine Report No. 6662, *Adaptive Nonlinear Coherent Processor Design*, Final Technical Report for Rome Air Development Center, USAF, Report No. RADC-TR-89-387, 1990.

[10] J. H. Higbie, "Adaptive Nonlinear Suppression of Interference," *Proceedings of the 1988 IEEE MILCOM Conference*, pp. 23.3.1-9, 1988.

[11] J. G. Proakis, *Digital Communications*, Second Edition, New York: McGraw-Hill, 1989.

[12] H. Stark and J. Woods, *Probability, Random Processes, and Estimation Theory for Engineers*, Second Edition, Englewood Cliffs, NJ: Prentice-Hall, 1994.

[13] E. Kreyszig, *Advanced Engineering Mathematics*, Sixth Edition, New York: John Wiley and Sons, 1988.

[14] D. W. Scott, *Multivariate Density Estimation: Theory, Practice, and Visualization*, New York: John Wiley and Sons, 1992.

Additional References Concerning Locally Optimum Detection

[15] R. S. Blum and S. A. Kassam, "Optimum Distributed Detection of Weak Signals in Dependent Sensors," *IEEE Transactions on Information Theory*, Vol. 38, No. 3, pp. 1066-1079, May 1992.

[16] D. M. Hummels and J. Ying, "Locally Optimum Detection of Unknown Signals in Non-Gaussian Markov Noise," *IEEE Midwest Symposium on Circuits and Systems*, pp. 1098-1101, 1991.

[17] J. F. Kuehls and E. Geraniotis, "Memoryless Locally Optimum Detection of Rate Lines," *Proceedings of the 1990 IEEE MILCOM Conference*, pp. 812-816, 1990.

[18] A. M. Maras, "Locally Optimum Bayes Detection in Ergodic Markov Noise," *IEEE Transactions on Information Theory*, Vol. 40, No. 2, pp. 41-55, January 1994.

*(9) RADC-TR-89-387 is Distribution limited to DOD and DOD contractors only, premature dissemination.

[19] A. B. Martinez and J. B. Thomas, "Detector Design Using a Density Fit to Non-Gaussian Noise," *IEEE Transactions on Information Theory,* Vol. 34, No. 3, pp. 544-550, May/June 1988.

[20] A. B. Martinez, et. al., "Locally Optimal Detection in Multivariate Non-Gaussian Noise," *IEEE Transactions on Information Theory,* Vol. IT-30, No. 6, pp. 815-822, November 1984.

[21] H. V. Poor, *An Introduction to Signal Detection and Estimation,* New York: Springer-Verlag, 1988.

[22] I. Song and S. A. Kassam, "Locally Optimum Detection of Signals in a Generalized Observation Model: The Known Signal Case," *IEEE Transactions on Information Theory,* Vol. 36, No. 3, pp. 502-515, May 1990.

[23] I. Song and S. A. Kassam, "Locally Optimum Detection of Signals in a Generalized Observation Model: The Random Signal Case," *IEEE Transactions on Information Theory,* Vol. 36, No. 3, pp. 516-530, May 1990.

[24] I. Song and S. A. Kassam, "Locally Optimum Rank Detection of Correlated Random Signals in Additive Noise," *IEEE Transactions on Information Theory,* Vol. 38, No. 4., pp. 1311-1322, July 1992.

[25] A. D. Spaulding, "Locally Optimum and Suboptimum Detector Performance in a Non-Gaussian Interference Environment," *IEEE Transactions on Communications,* Vol. COM-33, No. 6, pp. 509-517, July 1985.

[26] A. D. Spaulding and D. Middleton, "Optimum Reception in an Impulsive Interference Environment - Part I: Coherent Detection," *IEEE Transactions on Communications,* Vol. COM-25, No. 9, pp. 910-923, September 1977.

MISSION
OF
ROME LABORATORY

Mission. The mission of Rome Laboratory is to advance the science and technologies of command, control, communications and intelligence and to transition them into systems to meet customer needs. To achieve this, Rome Lab:

    a. Conducts vigorous research, development and test programs in all applicable technologies;

    b. Transitions technology to current and future systems to improve operational capability, readiness, and supportability;

    c. Provides a full range of technical support to Air Force Material Command product centers and other Air Force organizations;

    d. Promotes transfer of technology to the private sector;

    e. Maintains leading edge technological expertise in the areas of surveillance, communications, command and control, intelligence, reliability science, electro-magnetic technology, photonics, signal processing, and computational science.

The thrust areas of technical competence include: Surveillance, Communications, Command and Control, Intelligence, Signal Processing, Computer Science and Technology, Electromagnetic Technology, Photonics and Reliability Sciences.